

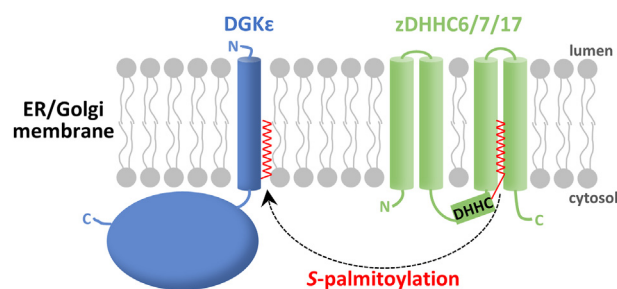
Diacylglycerol kinase- ϵ is S-palmitoylated on cysteine in the cytoplasmic end of its N-terminal transmembrane fragment

Gabriela Traczyk^{*ID}, Aneta Hromada-Judycka^{*ID}, Anna Świątkowska^{ID}, Julia Wiśniewska^{ID}, Anna Ciesielska^{ID}, and Katarzyna Kwiatkowska^{*ID}

Laboratory of Molecular Membrane Biology, Nencki Institute of Experimental Biology PAS, Warsaw, Poland

Abstract Diacylglycerol kinase- ϵ (DGK ϵ) catalyzes phosphorylation of diacylglycerol to phosphatidic acid with a unique specificity toward 1-stearoyl-2-arachidonoyl-*sn*-glycerol, which is a backbone of phosphatidylinositol (PI). Owing to this specificity, DGK ϵ is involved in the PI cycle maintaining the cellular level of phosphorylated PI derivatives of signaling activity and was also found crucial for lipid metabolism. DGK ϵ dysfunction is linked with the development of atypical hemolytic uremic syndrome (aHUS) and possibly other human diseases. Despite the DGK ϵ significance, data on its regulation by cotranslational and/or post-translational modifications are scarce. Here, we report that DGK ϵ is S-palmitoylated at Cys38/40 (mouse/human DGK ϵ) located in the cytoplasmic end of its N-terminal putative transmembrane fragment. The S-palmitoylation of DGK ϵ was revealed by metabolic labeling of cells with a palmitic acid analogue followed by click chemistry and with acyl-biotin and acyl-polyethylene glycol exchange assays. The S-acyltransferases zDHHC7 (zinc finger DHHC domain containing) and zDHHC17 and the zDHHC6/16 tandem were found to catalyze DGK ϵ S-palmitoylation, which also increased the DGK ϵ abundance. Mouse DGK ϵ -Myc ectopically expressed in human embryonic kidney 293 cells localized to the endoplasmic reticulum where zDHHC6/16 reside and in small amounts also to the Golgi apparatus where zDHHC7 and zDHHC17 are present. The Cys38Ala substitution upregulated, whereas hyperpalmitoylation of wild-type DGK ϵ reduced the kinase activity, indicating an inhibitory effect of the Cys38 S-palmitoylation. In addition, the substitution of neighboring Pro31 with Ala also diminished the activity of DGK ϵ . Taken together, our data indicate that S-palmitoylation can fine-tune DGK ϵ activity in distinct cellular compartments, possibly by affecting the distance between the kinase and its substrate in a membrane.

Supplementary key words atypical hemolytic uremic syndrome • cell signaling • diacylglycerol kinase • kinase activity assay • lipids/chemistry • palmitoylation • phosphoinositides • zDHHC



Diacylglycerol kinases (DGKs) catalyze phosphorylation of diacylglycerol (DAG) to phosphatidic acid (PA). Ten mammalian DGK isoenzymes, α - κ , have been identified and classified into five groups depending on their structure. They all contain two (or three) cysteine-rich conserved homology-1 (C1)-like domains and a catalytic and an accessory domain, but their regulatory domains differ (1, 2). Diacylglycerol kinase- ϵ (DGK ϵ) is unique among them—it lacks regulatory domains and is thought to be incorporated into a membrane by a hydrophobic fragment comprising 21 amino acids near its N terminus (residues 22–42 in human DGK ϵ [hDGK ϵ] and 20–40 in mouse DGK ϵ [mDGK ϵ]) that is highly conserved in vertebrates (3, 4). DGK ϵ is also distinguished from other DGKs by its specificity toward DAG bearing C16:0 or C18:0 and C20:4 fatty acids at the *sn*-1 and *sn*-2 position, respectively (5–8). The C18:0/20:4 DAG (SAG) is the backbone of phosphatidylinositol (PI) and its phosphorylated derivatives; therefore, DGK ϵ is presumed to contribute to the so-called PI cycle together with phosphatidate cytidylyltransferase 2 converting the PA into CDP-DAG (9). This enzymatic cycle serves to rebuild the cellular PI pool following the

*These authors contributed equally to this work.

*For correspondence: Katarzyna Kwiatkowska, kkwiatkowska@nencki.edu.pl.

hydrolysis of PI(4,5)P₂ in the course of signal transduction by a large number of plasma membrane receptors. Recent data indicate, however, that at a DGK ϵ deficiency, the PI turnover triggered by PI(4,5)P₂ hydrolysis still occurs, indicating that the specific fatty acyl chain composition of PI and its phosphorylated derivatives can result from an involvement of other DGKs combined with the remodeling of the fatty acyl chains in the so-called Lands' cycle (10). The interest in DGK ϵ is enhanced by the link detected in mouse models between its activity and the development of Huntington's disease, seizure susceptibility, and protection from obesity (11–13). Importantly, mutations of *DGKE* are linked with the atypical hemolytic uremic syndrome (aHUS) in humans ((14); see <https://bibliome.ai/hg19/gene/DGKE> for current update). Some of those abnormalities have been correlated with changes in PI(4,5)P₂ turnover (11, 15).

These features make DGK ϵ of significant interest, but the complexity of its regulatory mechanisms is only beginning to be elucidated. Thus, although DGK ϵ contains the CIA and CIB domains resembling those which bind DAG in conventional and novel protein kinase C isoforms, SAG binds to the lipoxigenase-like motif of DGK ϵ rather than to those domains (16, 17). On the other hand, the CI domains can interact with the catalytic domain of DGK ϵ (4, 18) and codetermine its substrate specificity, in analogy to DGK α (8). Our group found recently that the activity and stability of DGK ϵ depend on the zinc finger motif present in the CIB domain. Substitution of any of the cysteines or the histidine of this motif, notably found in some aHUS patients, inactivates the kinase and leads to its proteasomal degradation (19). Finally, the activity and substrate specificity of DGK ϵ are upregulated allosterically by membrane morphology, that is, by negatively curved membranes, as found examining purified hDGK ϵ and liposomes of various compositions and sizes (20). The latter suggests that DGK ϵ functioning can depend on its localization in specific regions of cellular membranes.

S-palmitoylation is one of the factors that contribute to the accumulation of proteins, both transmembrane and peripheral ones, in selected domains of cellular membranes, including membranes of the endoplasmic reticulum, Golgi apparatus, and the plasma membrane (21–25). This post-translational modification consists the attachment of a palmitic acid residue to the sulfhydryl group of cysteine via a thioester bond and is potentially reversible. It is catalyzed by S-acyltransferases from the zinc finger DHHC domain containing (zDHHC) protein family, comprised of 23 enzymes in mammals (26–28). We have recently discovered that DGK ϵ is palmitoylated, and the amount of such modified protein increases in Raw264 macrophage-like cells after lipopolysaccharide stimulation (29). It has been established that proteins can be acylated with fatty acids other than palmitic acid, and on rare occasions, the acyl chain can be attached to amino acids other than

cysteine (30). Therefore, drawing on recent methodological progress in this work, we continued studies on DGK ϵ acylation. The click chemistry-based technique requires metabolic labeling of cells with a fatty acid analogue bearing an alkyne (or azide) moiety at the omega carbon. After cell lysis, the acylated proteins are detected by a “click” reaction between the alkyne (or azide) and an azide (or alkyne) residue of a reporter tag, either biotin or a fluorescent dye. This technique does not discriminate between S-acylation of cysteine and the rare *O*- and ϵ -*N*-acylation at serine or threonine and lysine, respectively (31, 32). On the other hand, the acyl-biotin exchange (ABE) technique relies on the substitution of a thiol-bound fatty acid with a thiol-reactive biotin derivative; hence, it only detects S-acylation, including S-palmitoylation (33). However, it can give false-positive results by detecting proteins forming a thioester linkage with moieties other than fatty acids, like some enzymes of the ubiquitination cascade forming thioester intermediates with ubiquitin (34).

Taking into account the pros and cons of the click-based chemistry and ABE, we used both these techniques to study the S-palmitoylation of DGK ϵ and identified Cys38/40 (mDGK ϵ /hDGK ϵ) as the site of this modification. We also found that DGK ϵ can be S-palmitoylated by zDHHC6/16, zDHHC7, and zDHHC17, and that this modification downregulates DGK ϵ activity.

MATERIALS AND METHODS

Plasmids

Complementary DNA of mDGK ϵ (NM_019505) was obtained and cloned into the pcDNA3.1/Hygro(+) vector (Invitrogen) and fused with a double Myc tag at the C terminus, as described by Traczyk *et al.* (19). Plasmid encoding hDGK ϵ (NM_003647) was purchased from OriGene (catalog no.: RC219913). The *DGKE* coding sequence was subcloned into the pcDNA3.1/Hygro(+)-2xMyc vector using primers: forward 5'-CTTTCTAGAACCATGGAAGCGGAGAGGCG-3' and reverse 5'-CTTTCTAGATTTCAGTCGCCCTTTATATCTTCTTGA-3' and XbaI restriction enzyme to obtain hDGK ϵ doubly Myc tagged at the C terminus. mDGK ϵ /hDGK ϵ mutant forms were prepared by site-directed mutagenesis; all wild-type and mutant m/hDGK ϵ -Myc constructs were verified by sequencing (Genomed SA). Primers used for *Dgke* and *DGKE* mutagenesis are listed in supplemental Table S1. A library of pEF-BOS-hemagglutinin (HA) plasmids encoding HA-tagged mouse DHHC1-DHHC23 S-acyltransferases and glutathione-S-transferase (GST) for control were obtained from Prof Masaki Fukata (National Institute of Physiological Sciences, Okazaki, Japan; (26, 35)).

Cell culture and transfection

Human embryonic kidney 293 (HEK293) cells (American Type Culture Collection CRL-1573™, mycoplasma free) were plated at 1.2×10^6 in a 6 cm dish (for click, ABE, and acyl-polyethylene glycol [PEG] exchange [APE]) or 0.5×10^6 in a 3.5 cm dish (for activity measurements and

immunofluorescence studies). After 24 h, the cells were transfected with 2 μ g (for click and ABE in experiments with no ectopic expression of *S*-acyltransferases) or 850 ng (for activity measurements and immunofluorescence studies) of pcDNA3.1/Hygro(+) plasmids encoding wild-type mDGK ϵ or hDGK ϵ or their mutants in 3.3 ml or 1.5 ml DMEM containing 4.5 g/l glucose and 10% FBS, and supplemented with FuGENE HD (Promega) in the ratio 4:1 to the amount of DNA (μ l: μ g) according to the manufacturer's instruction. To identify the zDHHC *S*-palmitoylating DGK ϵ , cells (1.2×10^6 in a 6 cm dish) were transfected with 1 μ g (ABE) or 2 μ g (APE) of pcDNA3.1/Hygro(+) plasmid encoding wild-type mDGK ϵ -Myc together with 1 μ g (ABE) or 2 μ g (APE) of pEF-BOS-HA plasmid bearing one of the 23 *Zdhhc* genes or *Gst* in 3.3 ml DMEM/glucose/FBS using FuGENE HD, as above. In a series of experiments, pcDNA-mDGK ϵ -Myc was cotransfected with pEF-BOS-HA plasmids encoding zDHHC6-HA and zDHHC16-HA (1 μ g each/dish). Also, when indicated, the plasmids encoding mDGK ϵ -Myc or zDHHC-HA were substituted with respective amounts of empty pcDNA3.1 Hygro(+) vector. For the kinase activity measurements in cells coexpressing mDGK ϵ -Myc and zDHHC17-HA, the proportion of respective plasmids was as for APE, that is, 850 ng each. Transfection was conducted for 24 h when coexpression of mDGK ϵ -Myc with zDHHC-HA was induced (35) or for 48 h for expression of DGK ϵ -Myc alone. In the latter case, the culture medium was exchanged after 24 h for DMEM containing glucose and FBS as above with 0.05 mg/ml streptomycin and 50 U/ml penicillin, and the cell cultivation was continued for additional 24 h. For immunofluorescence studies, after 24 h of transfection, cells were transferred onto coverslips for the remaining 24 h of the cultivation and used for protein localization as described below. In a series of experiments, MG-132 (Merck) was added to the culture medium after 30 h of transfection at 1 μ M for the remaining 18 h of the culture. For biochemical assays, the cells were harvested in cold PBS, pelleted, and stored at -80°C .

Click chemistry

After 48 h of transfection with wild-type mDGK ϵ -Myc or its mutants, HEK293 cells were incubated with 50 μ M 17-octadecynoic acid (17ODYA; Merck) added from stock solution in DMSO or with 0.05% DMSO in DMEM containing 2% charcoal-stripped FBS and 30 mM Hepes for 4 h at 37°C and processed essentially as described earlier (29). Briefly, harvested and pelleted cells were lysed in 300 μ l of lysis buffer containing 0.5% SDS, 0.5% NP-40, 100 mM NaCl, 50 mM phosphate buffer, pH 7.4, 1 mM TCEP (Tris(2-carboxyethyl)phosphine hydrochloride), protease inhibitors (1 mM PMSF, 2 μ g/ml aprotinin, 2 μ g/ml leupeptin, and 0.7 μ g/ml pepstatin), phosphatase inhibitor (1 mM Na_3VO_4), protein thioesterase inhibitors (10 μ M palmostatin and 0.2 mM 1-hexadecanesulfonyl fluoride), and 250 U/ml Benzonase Nuclease (Merck). After 30 min (4°C), the lysates were sheared by passing through a 25-G needle and clarified by centrifugation (4°C , 5 min, 14,500 g), and supernatants were diluted with five volumes of the lysis buffer without the detergents and TCEP, supplemented with 15 μ l of Myc-Trap Agarose (with anti-Myc alpaca antibody) (Chromotek; catalog no.: yta) and incubated for 3 h at 4°C with end-over-end rotation. Subsequently, samples were washed three times with ice-cold lysis buffer containing 0.05% NP-40 and once with lysis buffer without the detergent. Finally, the agarose beads were suspended in 50 μ l of click reaction mixture containing 100 mM NaCl, 10 μ M IRDye 800CW-

azide (LI-COR, Lincoln), 1 mM TCEP, 100 μ M Tris((1-benzyl-4-triazolyl)methyl)amine, 1 mM CuSO_4 , 50 mM phosphate buffer, pH 7.4, and protease inhibitors (cOmplete EDTA-free protease inhibitor cocktail [Roche], 1 mM PMSF, and 0.7 μ g/ml pepstatin). In a series of experiments, 5 mM methoxypolyethylene glycol azide (PEG-azide, Merck, catalog no.: 689475) was used for the click reaction. After 1 h in the darkness with gentle rotation, samples were washed with lysis buffer containing 0.05% NP-40, and agarose beads were suspended in 40 μ l of 2 \times SDS-sample buffer and heated for 10 min at 95°C . A subset of the 17ODYA-labeled samples were additionally incubated with 1 M hydroxylamine (HXA) for 30 min at 22°C and next diluted twice and incubated for 5 min at 100°C . Proteins were separated by 10% SDS-PAGE and analyzed in an Odyssey CLx Imager (LI-COR) and after that transferred onto nitrocellulose and subjected to immunoblotting.

ABE

The ABE technique was applied to detect *S*-palmitoylation of DGK ϵ essentially as described previously (36), with minor modifications. In brief, HEK293 cells were lysed in 500 μ l of 150 mM NaCl, 5 mM EDTA, 1.7% Triton X-100, 4% SDS, cOmplete protease inhibitor cocktail, 2 mM PMSF, 250 U/ml Benzonase Nuclease, 50 mM Tris, pH 7.2, for 15 min at 37°C with shaking, followed by sonication for 60 s (0.3 cycle; amplitude 33%; UP200S Hielscher sonifier). Lysate proteins were precipitated with chloroform:methanol: H_2O (1:4:3, v:v:v), dissolved in SDS buffer (4% SDS, 5 mM EDTA, 100 mM Hepes, pH 7.4) at 2 mg/ml, and incubated with 5 mM TCEP and 20 mM methyl methanethiosulfonate for 15 min at 37°C and 20 min at 50°C , respectively, and precipitated three times as above. For biotinylation, the protein pellet was dissolved in 150 μ l of the SDS buffer, diluted 20 times in a buffer containing 0.27 mM HPDP-biotin (ThermoFisher Scientific), 0.27% Triton X-100, and 100 mM Hepes, pH 7.4. Each sample was halved, supplemented either with 1 M HXA+ or with 50 mM Tris, pH 7.5 (HXA-), and incubated for 2 h at 20°C with agitation. Proteins were precipitated three times and solubilized as above, 20- μ g aliquots were withdrawn as input samples, whereas 300 μ g protein/sample was diluted 20 times in Triton buffer containing 150 mM NaCl, 0.2% Triton X-100, 20 mM Hepes, pH 7.4, 1 μ g/ml leupeptin, aprotinin, and pepstatin, 1 mM PMSF, 1 mM Na_3VO_4 , 50 μ M phenylarsine oxide, and supplemented with 50 μ l of streptavidin-agarose (ThermoFisher Scientific). After 2 h of gentle agitation at 20°C , agarose beads were pelleted and washed three times in the Triton buffer without inhibitors. Finally, the beads were suspended in 150 μ l of elution buffer (150 mM NaCl, 0.2% SDS, 0.2% Triton X-100, 2% β -mercaptoethanol, 20 mM Hepes, pH 7.5) for 15 min (at 37°C with shaking) and subsequently in 100 μ l of 1 \times SDS-sample buffer for 5 min (at 95°C with shaking). The two eluates were combined, and proteins precipitated with four volumes of cold acetone, dissolved in 30 μ l of 2 \times SDS-sample buffer, denatured for 5 min at 95°C , and subjected to 10% SDS-PAGE.

APE

To reveal the number of *S*-acylated cysteine residues in DGK ϵ , the palmitic acid residue(s) of mDGK ϵ -Myc were exchanged for PEG in the APE technique (37), which in principle resembles ABE. For this, HEK293 cells overexpressing mDGK ϵ -Myc together with selected zDHHC-HA or GST for control (24 h) were lysed, and the lysates were incubated with

5 mM TCEP and 20 mM methyl methanethiosulfonate with subsequent protein precipitation, as described above. The protein pellet was dissolved in 220 μ l of the SDS buffer, protein concentration was adjusted to 2 mg/ml, and then diluted 20 times with a buffer containing 0.27% Triton X-100 and 100 mM Hepes, pH 7.4, halved, and supplemented or not with 1 M HXA (HXA+ or HXA-), and incubated for 2 h at 20°C with agitation. Protein was precipitated three times as above and finally dissolved in 100 μ l of the SDS buffer. The samples were next supplemented with 100 μ l of 4 mM methoxypolyethylene glycol maleimide (PEG-maleimide) (M_n 5,000; Merck, catalog no.: 63187) in the SDS buffer. After 2 h (20°C, with agitation), protein was precipitated three times and finally dissolved in 35 μ l of the SDS buffer. Protein concentration was determined, samples were supplemented with 12 μ l of 4 \times SDS-sample buffer, incubated for 5 min at 95°C, and subjected in equal amounts to 10% SDS-PAGE.

DGK ϵ activity determination

The DGK ϵ enzymatic activity was determined using mixed micelle assay according to our previous studies (19). For micelle preparation, 1-NBD-stearoyl-2-arachidonoyl-*sn*-glycerol (NBD-SAG, Cayman Chemical, catalog no.: 10011300), SAG (Cayman Chemical, catalog no.: 10008650), and 1,2-diacyl-*sn*-glycerophosphoserine (PS, Merck, catalog no.: P7769) dissolved in chloroform:methanol (2:1, v:v, with 30 μ g/ml butylated hydroxytoluene as an antioxidant) were mixed at a 5:7 molar ratio of total SAG:PS. The total SAG contained 10% of NBD-SAG. The lipid mixture was dried and resuspended by vortexing (2 min, room temperature) in 4 \times reaction buffer containing 400 mM NaCl, 80 mM MgCl₂, 4 mM EGTA, 4 mM DTT, 300 mM octyl- β -glucoside, 200 mM Mops, pH 7.2, and supplemented with 2 mM ATP. Obtained micelles were used to determine mDGK ϵ -Myc activity in homogenates and detergent lysates of HEK293 cells and in mDGK ϵ -Myc immunoprecipitates. For homogenization, HEK293 cells 48 h after transfection with mDGK ϵ -Myc alone were suspended in 300 μ l of ice-cold homogenization buffer (0.25 M sucrose, 1 mM EDTA, 4 mM EGTA, 1 mM DTT, 20 mM Tris-HCl, pH 7.4, with 1 mM PMSF, 0.7 μ g/ml pepstatin, 20 μ g/ml aprotinin, and 20 μ g/ml leupeptin) and sonicated, as described (19). For lysis and immunoprecipitation, HEK293 cells 24 h after transfection were used since this time was optimal for coexpression of mDGK ϵ -Myc and zDHHCl7-HA, as described above. Cells were lysed essentially as described (19) at 4°C in 150 μ l of lysis buffer supplemented with 1 mM DTT (150 mM NaCl, 20 mM Tris-HCl, pH 7.4, 1% NP-40, 1 mM EDTA, 1 mM DTT, 1 mM PMSF, 20 μ g/ml aprotinin, and 20 μ g/ml leupeptin) and sonicated as above. Then lysates were clarified by centrifugation (4°C, 3 min, 12,500 g), and supernatants were used for the kinase activity measurements or subjected to mDGK ϵ -Myc immunoprecipitation. For the latter, 150 μ g of total lysate protein was supplemented with 30 μ l of the Myc-Trap Agarose and incubated for 3 h at 4°C with rotation. After washing, the Myc-Trap Agarose with bound mDGK ϵ -Myc was divided in half, and one half was resuspended in 40 μ l of lysis buffer supplemented with 0.25 M sucrose and 4 mM EGTA and used for the kinase activity assay; the other half was used for immunoblotting (19). For the activity assay, 15 μ g of total protein in 40 μ l of homogenization buffer or in lysis buffer (containing 0.25 M sucrose and 4 mM EGTA) or half of the mDGK ϵ -Myc immunoprecipitate described above was added to the reaction mixture containing 50 μ l of 4 \times reaction buffer with micelles and 110 μ l of H₂O. The final concentration of NBD-SAG/SAG in the reaction mixture was 1.45 or 4.46 mol% (0.75 mM or 2.5 mM) and of PS 2.03 or

6.25 mol% (1.05 mM or 3.5 mM). The DGK ϵ activity assay was carried out for 10 min at 24°C with gentle agitation and stopped by the addition of 1 ml of methanol followed by 1 ml of chloroform and 0.7 ml of 1% perchloric acid. After phase separation, lower phase was washed two times with 2 ml of 1% perchloric acid and dried under a nitrogen stream. Lipids were dissolved in chloroform:methanol (2:1, v:v) and separated by TLC on silica gel 60 (Merck) along with a standard, 0.5–100 pmol of 1-palmitoyl-2-NBD-dodecanoyl-*sn*-glycero-3-phosphate (NBD-PDPA, Avanti, catalog no.: 810174), with chloroform:methanol:acetic acid 80% (65:15:5, v:v:v) as mobile phase. NBD-lipids, including 1-NBD-stearoyl-2-arachidonoyl-*sn*-glycero-3-phosphate (NBD-SAPA) produced by DGK ϵ , were visualized using G:Box (Syngene), and fluorescence intensity was assessed with ImageJ 1.53t (NIH) software using a standard curve drawn for NBD-PDPA and corrected by subtraction of background from samples transfected with empty vector. In parallel, a fraction of the cell homogenates and lysates were supplemented with 2% SDS, vortexed and incubated for 15 min, next supplemented with 1 \times SDS-sample buffer (final concentration), incubated again for 15 min, heated for 10 min at 95°C, and subjected to 10% SDS-PAGE. Also the other half of the mDGK ϵ -Myc immunoprecipitate was suspended in 60 μ l of 2 \times SDS-sample buffer and heated for 10 min at 95°C to release proteins from the affinity gel for SDS-PAGE. Alongside, 2–30 ng of GST-hDGK ϵ (SignalChem, catalog no.: D24-10G) was applied onto the gels. After transfer onto nitrocellulose, samples were subjected to immunoblotting with sheep anti-DGK ϵ antibody (R&D Systems) (supplemental Table S2).

DGK ϵ localization using immunofluorescence microscopy

HEK293 cells were transfected as described above and after 24 h were transferred onto coverslips (5 \times 10⁴ per 15 \times 15 mm coverslip) and cultured for additional 24 h. Cells were rinsed twice with ice-cold PBS buffer containing 0.5 mM MgCl₂ and 1 mM CaCl₂ and once with APHEM buffer (60 mM Pipes, 25 mM Hepes, 10 mM EGTA, 4 mM MgCl₂, pH 6.9) and fixed in 4% paraformaldehyde in APHEM for 15 min at room temperature. Next, cells were washed with APHEM and incubated with 50 mM NH₄Cl/APHEM (10 min, room temperature) to block free aldehyde groups. After rinsing with APHEM buffer, cells were permeabilized with 0.05% Triton X-100 in TBS buffer (25 mM Tris-Cl, 130 mM NaCl) for 5 min on ice. To visualize the Golgi apparatus, the protocol described in (38) was used with minor modifications. Cells were permeabilized with 0.005% digitonin in APHEM for 10 min at room temperature and rinsed twice with TBS and incubated with 5% BSA in TBS for 30 min at room temperature. Subsequently, cells were incubated overnight at 4°C in 0.2% BSA/TBS with the following antibodies: anti-Myc mouse IgG (Cell Signaling, catalog no.: 2276) for mDGK ϵ -Myc staining and anti-STIM1 rabbit IgG (Cell Signaling, catalog no.: 5668) or anti-golgin-97 rabbit IgG (Cell Signaling, catalog no.: 13192) or anti-GM130 rabbit IgG (Cell Signaling, catalog no.: 12480). After five washes in 0.2% BSA/TBS, a 1 h incubation with secondary antibodies in 0.2% BSA/TBS was conducted at room temperature. The secondary antibodies used were donkey anti-mouse IgG-Alexa Fluor 647 (ThermoFisher Scientific, catalog no.: A-31571) and donkey anti-rabbit IgG-FITC (Jackson ImmunoResearch, catalog no.: 711-095-152); they were supplemented with 2 μ g/ml Hoechst 33342 (Merck, catalog no.: B2261). All the antibodies used are listed in supplemental Table S2. Cells were washed five times with 0.2% BSA/TBS and postfixed in 2% paraformaldehyde in PBS for 5 min at room temperature, washed three times with

PBS containing 50 mM NH₄Cl, once with 0.2% BSA/TBS, once with water, and embedded in Mowiol (Polysciences, catalog no.: 9002-89-5) containing antifading agent DABCO (Merck). Cells were examined under an LSM800 inverted confocal microscope (Zeiss) using a 63× oil objective (numerical aperture 1.4) with scan frame 898 × 898, speed 8, zoom 1.6, line averaging 2, pixel size 71 nm, and z interval 230 nm. Triple-stained images were obtained by sequential scanning for each channel to eliminate the crosstalk of the chromophores and to ensure a reliable quantification of colocalization. FITC fluorescence was excited at 488 nm, Alexa Fluor 647 at 640 nm, and Hoechst at 405 nm, and detected at 485–540, 637–700, and 400–487 nm, respectively. Images were processed using ImageJ software and finally were exported and maintained as TIFF images for figure preparation.

For analysis of colocalization, about 30 cells were analyzed from two independent transfections. For this, 16 bit z-stacks were used to build 3D structures with Imaris 10.0.1 (Oxford Instruments) software. Next, regions of interest (ROI) were selected on the basis of the staining for DGKε-Myc, STIM1, GM130, or golgin-97 using the surface detection algorithm of Imaris with 220 voxels for GM130 and golgin-97 or 10 voxels for DGKε-Myc and STIM1, and with a manually adjusted threshold. The background threshold values were identical for all images analyzed for the pair of analyzed proteins in a given experiment. To estimate the colocalization of mDGKε-Myc in its 3D ROI with a marker protein in the respective ROI, Manders' colocalization coefficient was used that measures co-occurrence of fluorescence independently of the signal proportionality (39).

SDS-PAGE and immunoblotting

Proteins were separated by SDS-PAGE and electrotransferred onto nitrocellulose, incubated with antibodies, and processed for detection by chemiluminescence as described previously (19, 29, 40). The following antibodies were used: sheep anti-DGKε (R&D Systems, catalog no.: AF7069), mouse anti-Myc (ThermoFisher, catalog no.: R950-25), mouse anti-CD71 (transferrin receptor, Santa Cruz Biotechnology, catalog no.: sc-32272), rabbit anti-Jak1 (Cell Signaling, catalog no.: 3344), mouse anti-actin (BD Transduction Laboratories, catalog no.: 612657), rabbit anti-flotillin-2 (Cell Signaling, catalog no.: 3436), donkey anti-sheep IgG-HRP (Jackson ImmunoResearch, catalog no.: 713-035-003), mouse anti-HA IgG-HRP (Cell Signaling, catalog no.: 2999), goat anti-mouse IgG-HRP (Jackson ImmunoResearch, catalog no.: 115-035-146), and goat anti-rabbit IgG-HRP (Merck, catalog no.: 401315 or Rockland, catalog no.: 611-1302). All the antibodies used are listed in supplemental Table S2. Visualized bands were analyzed densitometrically using the ImageJ program. Absorbance values were corrected by background subtraction, which in the case of click chemistry included samples incubated with DMSO.

Data analysis

Student's *t*-test was used for the statistical analysis of data. Data are represented as individual points and mean ± SD.

RESULTS

Cys 38/Cys40 is the major site of S-palmitoylation of mDGKε/hDGKε

In order to determine whether DGKε is palmitoylated, we cloned the *Dgke/DGKE* complementary DNAs

and modified them by adding the Myc tag at the C terminus of the encoded proteins. We decided on such a location of the tag because amino acids 20–40/22–42 (mDGKε/hDGKε) from the N terminus are predicted to form either a transmembrane or a U-shaped α-helix with Pro31/33 serving as a hinge (9) (Fig. 1A). Mouse DGKε-Myc was overexpressed in HEK293 cells, and its palmitoylation was revealed by metabolic labeling with 17ODYA, a palmitic acid analogue subsequently tagged with a fluorescent dye by click chemistry (Fig. 1B). Strong fluorescence of mDGKε-Myc was observed following its immunoprecipitate separation by SDS-PAGE for 17ODYA-labeled cells, which was virtually absent in a sample from mock-labeled cells (DMSO added instead of 17ODYA) (Fig. 1C, D). An equally negligible mDGKε-Myc fluorescence was observed in another control sample in which the lysate of cells metabolically labeled with 17ODYA was treated with HXA cleaving the thioester bond (supplemental Fig. S1A–C). The efficient removal of 17ODYA from mDGKε-Myc by HXA indicated that mDGKε undergoes S-palmitoylation. In full agreement, an S-acylation of mDGKε-Myc was also found with the ABE technique, which allows a selective capture of S-acylated proteins after substitution of their fatty acid residue(s) with biotin and enrichment on streptavidin beads (Fig. 1E–G). As expected, no mDGKε-Myc was detected in eluates from streptavidin beads incubated with samples not exposed to HXA, which had precluded the biotinylation of originally S-acylated proteins (Fig. 1F).

To identify the site(s) of the S-palmitoylation of DGKε, we focused on its N-terminal region, unique among all DGK isoenzymes and likely forming a transmembrane α-helix (4). We reasoned that cysteine residue(s) located in the membrane-associated fragment are the most likely sites of DGKε S-palmitoylation; therefore, Cys26 or Cys38 of mDGKε-Myc were substituted with Ala (Fig. 1A). The Cys38Ala substitution nearly fully abolished the S-palmitoylation of mDGKε-Myc, as found with click chemistry and ABE. The trace S-acylation represented less than 7% of that found for wild-type mDGKε (Fig. 1C, D, F, G). In contrast to Cys38Ala, the Cys26Ala mutation did not affect the S-palmitoylation of mDGKε-Myc (Fig. 1C, D, F, G). These data indicate that mDGKε is S-palmitoylated nearly exclusively at Cys38. Importantly, also hDGKε was found with the ABE assay to be S-palmitoylated, and Cys40 (corresponding to Cys38 in mDGKε) was identified as the site of this acylation, as evidenced by its abolishment by the Cys40Ala substitution (Fig. 1H).

Two other cysteine residues, Cys132 and Cys135, located in the CIB domain of mDGKε, had earlier been suggested as sites of its S-palmitoylation by a global analysis of the protein S-palmitoylation sites in mouse forebrain (41). We therefore mutated either of them and found that the Cys132Ala mutation did not affect the S-palmitoylation of mDGKε, whereas Cys135Ala led to its significant augmentation detected with both click

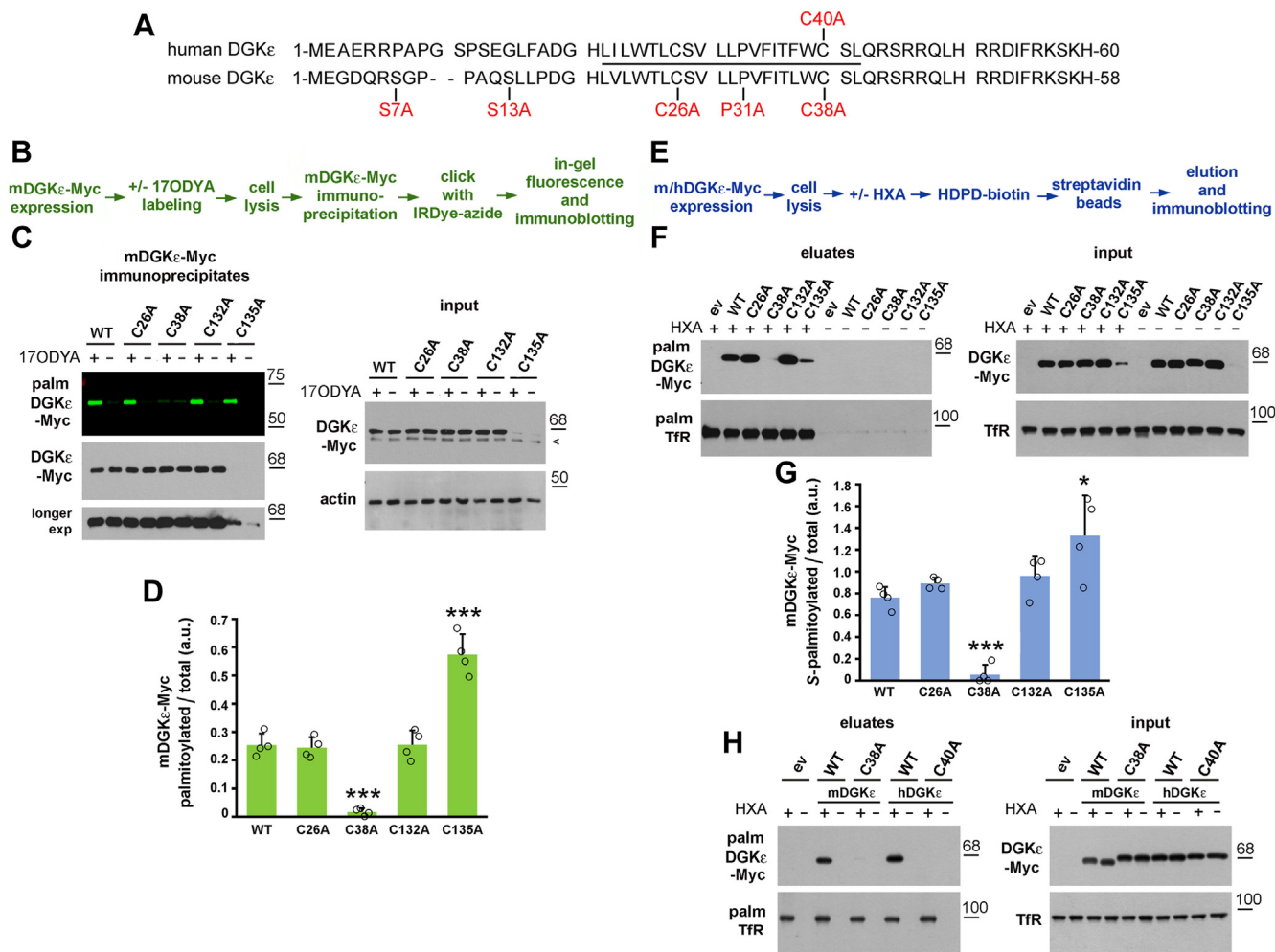


Fig. 1. DGK ϵ is S-palmitoylated at the cysteine located at the cytosolic end of its N-terminal transmembrane fragment. **A:** The amino acid sequence of the N-terminal fragment of hDGK ϵ and mDGK ϵ . Amino acids mutated in this study are indicated by red font. The predicted transmembrane fragment is indicated by the solid line. The complete mDGK ϵ /hDGK ϵ consists of 564/567 amino acids. **B:** Scheme of the click chemistry procedure. **C, D, F–H:** HEK293 cells were transfected with plasmid encoding WT mDGK ϵ -Myc (**C, D, F, G**) or hDGK ϵ -Myc (**H**) or their indicated mutant forms. **C, D:** After 48 h, cells were subjected to metabolic labeling with 50 μ M 17ODYA or exposed to 0.05% DMSO carrier as control (–17ODYA) for 4 h and lysed. mDGK ϵ -Myc was immunoprecipitated with anti-Myc alpaca antibody and subjected to click chemistry reaction with IRDye 800CW-azide. **C, upper panel:** In-gel fluorescence showing mDGK ϵ -Myc labeling with 17ODYA followed by IRDye-azide. **C, lower panels:** Efficiency of immunoprecipitation determined by immunoblotting with mouse anti-Myc antibody. The content of mDGK ϵ -Myc and actin in input lysates is shown on the right. Arrowhead indicates a band recognized unspecifically by the anti-Myc antibody. **D:** The extent of mDGK ϵ -Myc palmitoylation. mDGK ϵ -Myc fluorescence was determined by densitometry and normalized against the content of respective Myc-tagged DGK ϵ variant in immunoprecipitates. **E:** Scheme of the ABE procedure. **F–H:** After 48 h of transfection, cells were lysed and proteins were subjected to the ABE procedure involving treatment with HXA (HXA+) or not (HXA–), biotinylation, and capture of originally S-palmitoylated proteins on streptavidin-agarose beads. **F, H, upper panels:** S-palmitoylated mDGK ϵ -Myc (**F**) and hDGK ϵ -Myc (**H**) eluted from the streptavidin-agarose beads revealed with mouse anti-Myc antibody. **F, H, lower panels:** Transferrin receptor (Tfr), an Sacylated protein, eluted from the beads. The content of total mDGK ϵ -Myc, hDGK ϵ -Myc, and Tfr in input lysates is shown on the right. **G:** The extent of mDGK ϵ -Myc S-palmitoylation. The content of mDGK ϵ -Myc in eluates and input lysates was determined by densitometry, normalized against Tfr, and the ratio of S-palmitoylated mDGK ϵ -Myc (eluates) to total mDGK ϵ -Myc (lysates) is shown. Molecular weight markers in kDa are shown on the right. Data shown are mean \pm SD from four experiments. *, ***, Significantly different at $P=0.05$ and $P<0.001$, respectively, from cells expressing WT DGK ϵ . ev, empty vector.

chemistry and ABE (Figs. 1C, D, F, G and 2). We have recently found that Cys135 is an element of a zinc finger motif crucial for mDGK ϵ activity and stability, and its substitution with Ala leads to proteasomal degradation of the protein (19); indeed, the Cys135Ala mDGK ϵ -Myc variant was present in small quantities, which made its detection difficult (Figs. 1C, F and 2). In such conditions, the reliability of the quantitation of the

ratio of fluorescently or biotin-labeled to total mDGK ϵ -Myc protein amount is questionable; however, the hyperpalmitoylation of Cys135Ala mDGK ϵ -Myc was confirmed robustly when the amount of the Cys135Ala mDGK ϵ -Myc immunoprecipitate loaded on the gel was increased severalfold to equalize the amounts of Cys135Ala mDGK ϵ -Myc and wild-type mDGK ϵ -Myc (supplemental Fig. S2A–E).

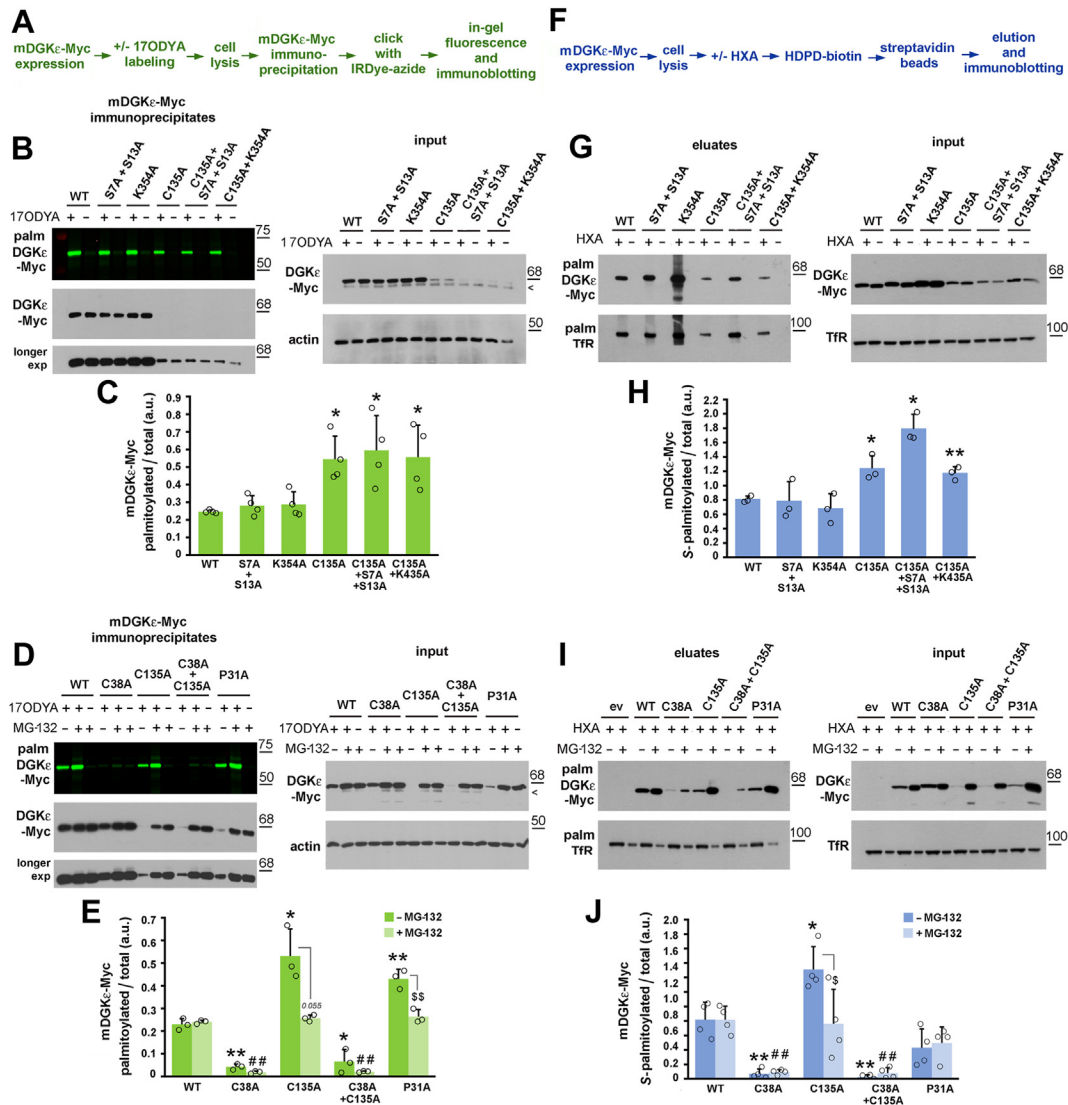


Fig. 2. Cys38 is the predominant site of mDGK ϵ S-palmitoylation. HEK293 cells were transfected with plasmid encoding WT mDGK ϵ -Myc or its indicated mutant forms and subjected to click chemistry or ABE. A: Scheme of the click chemistry procedure. B–E: After 48 h, cells were subjected to metabolic labeling with 50 μ M 17ODYA or exposed to 0.05% DMSO carrier as control (–17ODYA) for 4 h and lysed. D, E: When indicated, prior to lysis, cells were treated with the proteasomal inhibitor MG-132 (1 μ M, 18 h). mDGK ϵ -Myc was immunoprecipitated with anti-Myc alpaca antibody and subjected to click chemistry reaction with IRDye 800CW-azide. B, D, upper panels: In-gel fluorescence showing mDGK ϵ -Myc labeling with 17ODYA followed by IRDye-azide. B, D, lower panels: Efficiency of immunoprecipitation determined by immunoblotting with mouse anti-Myc antibody. The content of mDGK ϵ -Myc and actin in input lysates is shown on the right. Arrowheads indicate a band recognized unspecifically by the anti-Myc antibody. C, E: The extent of mDGK ϵ -Myc palmitoylation. mDGK ϵ -Myc fluorescence was determined by densitometry and normalized against the content of respective Myc-tagged DGK ϵ variants in immunoprecipitates. F: Scheme of the ABE procedure. G–J: After 48 h of transfection, cells were lysed and proteins subjected to the ABE procedure involving treatment with HXA (HXA+) or not (HXA–), biotinylation, and capture of originally S-palmitoylated proteins on streptavidin-agarose beads. I, J: When indicated, prior to lysis, cells were treated with MG-132 (1 μ M, 18 h). G, I, upper panels: S-palmitoylated mDGK ϵ -Myc eluted from streptavidin-agarose beads revealed with mouse anti-Myc antibody. G, I, lower panels: Transferrin receptor (Tfr), an S-acylated protein, eluted from the beads. The content of total mDGK ϵ -Myc and Tfr in input lysates is shown on the right. I: MG-132-treated samples were loaded at half the amount of protein from nontreated samples to avoid overloading. H, J: The extent of mDGK ϵ -Myc S-palmitoylation. The content of mDGK ϵ -Myc in eluates and input lysates was determined by densitometry, normalized against Tfr, and the ratio of S-palmitoylated mDGK ϵ -Myc (eluates) to total mDGK ϵ -Myc (lysates) is shown. Molecular weight markers in kDa are shown on the right. Data shown are mean \pm SD from four (C, J) or three (E, H) experiments. * and **, and #, ##, and §§, significantly different at $P < 0.05$ and $P < 0.01$, respectively, from cells expressing WT mDGK ϵ -Myc (*, **), WT mDGK ϵ -Myc in MG-132-treated cells (##). (*, §§) indicate the significance of difference between MG-132-treated and untreated cells. ev, empty vector.

To confirm further that the mDGK ϵ palmitoylation detected was indeed S-palmitoylation, the possibility of O-palmitoylation of mDGK ϵ at serine residues Ser7 and

Ser13 was investigated. These serine residues could be accessed by acyltransferases of the MBOAT family residing in the endoplasmic reticulum lumen (42, 43)

and hypothetically capable of catalyzing *O*-palmitoylation of DGK ϵ in a transmembrane conformation. Both Ser7 and Ser13 were substituted with Ala in wild-type or Cys135Ala mDGK ϵ -Myc. These mutations did affect neither palmitoylation of wild-type mDGK ϵ nor reduced the hyperpalmitoylation of Cys135Ala mDGK ϵ , as found using click chemistry (Fig. 2A–C and supplemental Fig. S2B, C) and ABE (Fig. 2F–H). These data argue against *O*-acylation of mDGK ϵ and indirectly confirm that we are dealing with *S*-palmitoylation, in agreement with the susceptibility of the mDGK ϵ -palmitate linkage to HXA treatment.

Next, we substituted Lys354 with Ala, as this residue can be ubiquitinated (9), which could affect mDGK ϵ *S*-palmitoylation, as has been observed for LRP6 (44). Again, no change of mDGK ϵ *S*-palmitoylation was caused by the Lys354Ala substitution, including the hyperpalmitoylation of Cys135Ala/Lys354Ala mDGK ϵ -Myc (Fig. 2B, C, G, H and supplemental Fig. S2B, C). Notably, the hyperpalmitoylation was nearly abolished in the double Cys38Ala/Cys135Ala mutant, indicating that it resulted from the *S*-palmitoylation of a larger fraction of mDGK ϵ at the “regular” site (Cys38) rather than from acylation of cysteine residue(s) other than Cys38 (Fig. 2D, E, I, J).

Finally, we substituted Pro31 implied to affect the conformation of the N terminus (4, 9) with Ala to assess its influence on DGK ϵ *S*-palmitoylation. The Pro31Ala substitution decreased the steady-state mDGK ϵ -Myc level (although to a lower extent than did the Cys135Ala substitution) and led to its hyperpalmitoylation; the latter was detected unequivocally with the click chemistry-based approach only (Fig. 2D, E and supplemental Fig. S2D, E). When the proteasomal activity was inhibited with MG-132, all mDGK ϵ forms were *S*-palmitoylated to a similar extent except for the barely modified Cys38Ala and Cys38Ala/Cys135Ala variants (Fig. 2D, E, I, J). Taken together, the data indicate that Cys38 is the predominant site of mDGK ϵ *S*-palmitoylation, and mDGK ϵ mutated at Cys135 or Pro31 (likely misfolded and rapidly degraded by 26S proteasome) can be hyperpalmitoylated.

zDHHC7 and zDHHCl7 can *S*-palmitoylate DGK ϵ

Having detected the *S*-palmitoylation of mDGK ϵ at Cys38, we aimed to determine which of the 23 mouse zDHHC enzymes could catalyze this reaction. To this end, we overproduced mDGK ϵ -Myc together with each of these enzymes in HEK293 cells, and after performing the ABE reaction, the amount of mDGK ϵ -Myc eluted from streptavidin beads was compared with that in controls with GST or empty vector in place of zDHHC. The amount of mDGK ϵ -Myc recovered from the beads indicated the extent of its *S*-palmitoylation (Fig. 3A, B and supplemental Fig. S3A, B). Note that in Fig. 3, the original nomenclature of the Sacyltransferases as DHHC is maintained (26, 35), which uses numbering of individual isoenzymes largely coincident

with that preferred currently in the zDHHC nomenclature.

We found that the extent of *S*-palmitoylation of mDGK ϵ -Myc was enhanced significantly in the presence of DHHC7 or DHHCl7 (zDHHC7 and zDHHCl7, respectively). The amount of mDGK ϵ -Myc eluted from the beads in the presence of either Sacyltransferase increased by about 40% in comparison to the GST control (Fig. 3B, C). We found that at the same time also the amount of total mDGK ϵ -Myc protein found in the input cell lysates increased substantially, by 16% in the presence of zDHHC7 and by as much as 31% in the presence of zDHHCl7 (Fig. 3B), resembling the effect of zDHHC3, 7, and 17-catalyzed *S*-palmitoylation of sprouty-2 (45).

The results of the analyses are summarized in Fig. 4. We used endogenous Jak1 as a positive control for the recovery of *S*-palmitoylated proteins in all labeled samples (Fig. 3B). Jak1 is *S*-palmitoylated at two cysteine residues (46) and we assured that the level of *S*-palmitoylated endogenous Jak1 eluted from streptavidin beads or the total amount of the protein in input lysates were not affected by the overproduction of zDHHC7 or zDHHCl7 (supplemental Fig. S3C, D). Therefore, the increase of the *S*-palmitoylation of the overproduced mDGK-Myc by zDHHC7 or zDHHCl7 was still substantial when normalized to the amount of endogenous *S*-palmitoylated Jak1 found in the eluates (Fig. 4A). Furthermore, we took into account the increase of the total amount of mDGK-Myc (also normalized to Jak1) found in these conditions (Figs. 3D and 4B). As a consequence, the extent of mDGK ϵ -Myc *S*-palmitoylation, that is, the ratio of the amounts of *S*-palmitoylated mDGK ϵ -Myc and total mDGK ϵ -Myc protein increased marginally in the case of zDHHC7 or remained virtually unchanged for zDHHCl7 (Fig. 4C). Taken together, these results show that zDHHC7 and zDHHCl7, located in the Golgi apparatus (25), can carry out *S*-palmitoylation of mDGK ϵ (Fig. 4D).

zDHHC7, 17, and 6/16 *S*-palmitoylate mDGK ϵ at one cysteine residue

Next, we aimed to quantitate the fraction of the *S*-palmitoylated DGK ϵ and verify the number of the *S*-acylation sites. For this, HEK293 cells cotransfected with mDGK ϵ -Myc and selected zDHHCs-HA (or GST for control) were subjected to the APE assay, which relies on the substitution of cysteine-bound fatty acyls by the thiol-reactive PEG-maleimide leading to a stable PEGylation of the cysteines (37). The labeling of mDGK ϵ -Myc with PEG slows its gel migration allowing simultaneous detection of the labeled (originally *S*-palmitoylated) and nonmodified mDGK ϵ -Myc (Fig. 5A).

We focused on zDHHC7 and zDHHCl7 but, because DGK ϵ is localized to the endoplasmic reticulum (47, 48), we also included in those experiments zDHHC6 paired with zDHHCl6. zDHHC6 is located exclusively in the endoplasmic reticulum and catalyzes *S*-palmitoylation

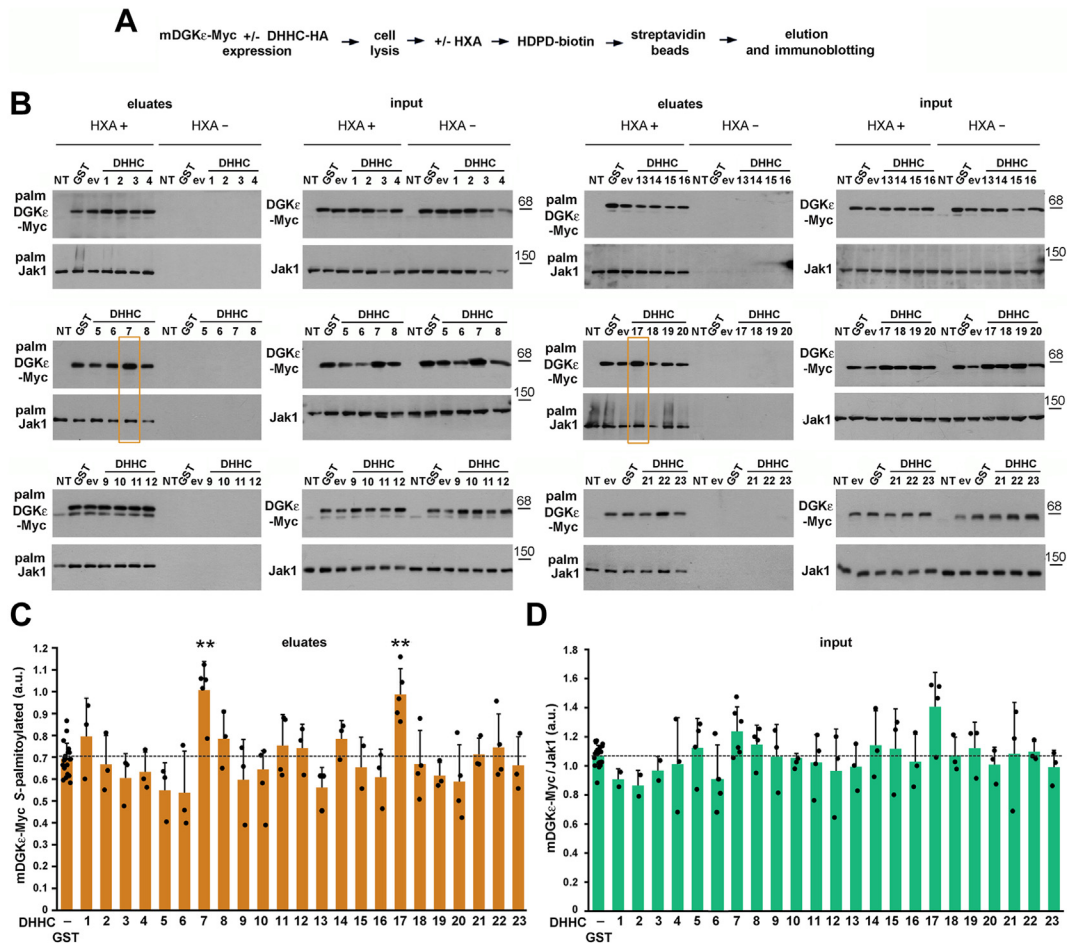


Fig. 3. DGK ϵ can be S-palmitoylated by zDHHC7 and zDHHC17. HEK293 cells were cotransfected with plasmids encoding WT mDGK ϵ -Myc and one of the mouse S-acyltransferases DHHC1-23 tagged with HA or with GST-HA or empty vector (ev) in controls. After 24 h, cells were lysed and proteins were subjected to the ABE procedure involving treatment with HXA (HXA+) or not (HXA-), biotinylation, and capture of originally S-palmitoylated proteins on streptavidin-agarose beads. **A:** Scheme of the ABE procedure. **B:** S-palmitoylated mDGK ϵ -Myc (upper panels) and Jak1 (lower panels) eluted from the streptavidin-agarose beads revealed with sheep anti-DGK ϵ and rabbit anti-Jak1 antibody, respectively. The content of mDGK ϵ -Myc and Jak1 in input lysates is shown on the right. A faint band seen in some panels below mDGK ϵ -Myc represents endogenous hDGK ϵ . Eluates obtained from cells coexpressing mDGK ϵ -Myc and DHHC7 or DHHC17 are boxed in yellow. **C:** The content of S-palmitoylated mDGK ϵ -Myc in eluates was determined by densitometry. **D:** The content of total mDGK ϵ -Myc in input lysates normalized against total Jak1. Molecular weight markers in kDa are shown on the right. Data shown are mean \pm SD, experiments in (D) were run in duplicates (HXA+ and HXA-). **, significantly different at $P < 0.01$ from cells coexpressing mDGK ϵ -Myc and GST-HA. **C, D:** The values for GST-expressing cells are averages for all samples tested while the significance of differences was evaluated by comparing values for cells expressing given DHHC with those from GST-expressing cells analyzed on the same gels. DHHC are numbered after Fukata *et al.* (26, 35), DHHC10, 11, 13, 22, and 23 correspond to zDHHC11, 23, 24, 13, and 25, respectively. NT, cells not transfected.

of several local proteins under the control of zDHHC16 (49). To facilitate the subsequent quantitative analyses, in the APE experiments, we used twice the amount of the mDGK ϵ -Myc- and zDHHC-encoding plasmids for transfection relative to that used in the earlier ABE quantitative experiments shown in Fig. 3.

We found that in cells expressing mDGK ϵ -Myc with the GST control, about 20% of the kinase was modified with PEG reflecting its S-palmitoylation by endogenous zDHHC(s) (Fig. 5B–D). Importantly, Cys38Ala mDGK ϵ -Myc was not PEGylated, indicating that Cys38 is the only site of mDGK ϵ S-palmitoylation (Fig. 5B). These results were confirmed using a different method—click chemistry between 17ODYA and PEG-azide

(supplemental Fig. S4A–C). In the presence of zDHHC7 or zDHHC17, two phenomena were detected—the amount of S-palmitoylated mDGK ϵ -Myc increased by as much as 5-fold above the GST control, which was accompanied by an increase in the abundance of nonpalmitoylated mDGK ϵ -Myc protein by about 65–80% (Fig. 5C, D). As a result, the fraction of PEGylated mDGK ϵ -Myc increased to about 41–46% of the total protein. Bearing in mind the higher levels of ectopically expressed mDGK ϵ -Myc and zDHHCs in the present experiments, their results are in broad agreement with those of the earlier ones obtained using different methods of analysis (Fig. 3). In the presence of zDHHC6/16, the increase in the abundance of

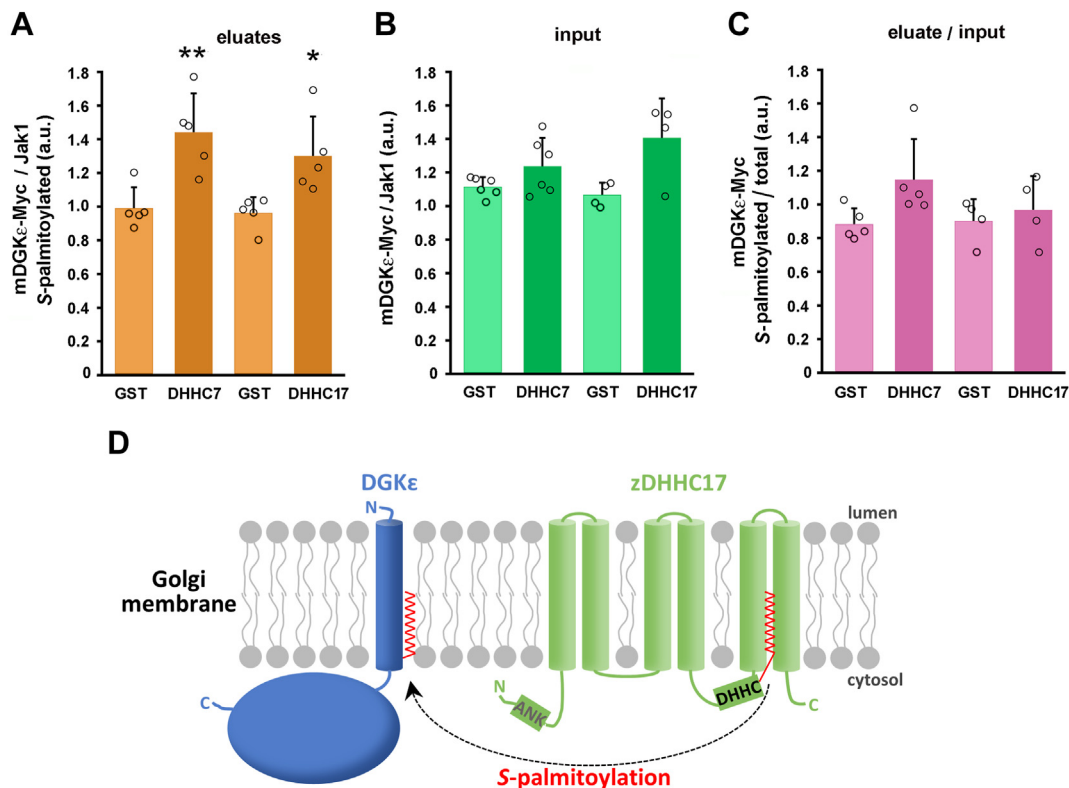


Fig. 4. DGK ϵ is S-palmitoylated by zDHHC7 and zDHHC17 with a concomitant increase of its abundance. HEK293 cells were cotransfected with plasmids encoding WT mDGK ϵ -Myc and zDHHC7 or zDHHC17 and analyzed as described in Fig. 3. A: The content of S-palmitoylated mDGK ϵ -Myc in eluates was determined by densitometry, as in Fig. 3, and normalized against S-palmitoylated Jak1. B: The content of total mDGK ϵ -Myc in input lysates normalized against total Jak1, as in Fig. 3. C: The extent of mDGK ϵ -Myc S-palmitoylation in cells coexpressing mDGK ϵ -Myc and zDHHC7 or zDHHC17. The content of mDGK ϵ -Myc in eluates and input lysates was normalized against Jak1, and the ratio of S-palmitoylated mDGK ϵ -Myc (eluates) to total mDGK ϵ -Myc (lysates) is shown. Data shown are mean \pm SD from at least four experiments. * and **, significantly different at $P < 0.05$ and $P < 0.01$, respectively, from cells coexpressing mDGK ϵ -Myc and GST-HA. D: Scheme of DGK ϵ S-palmitoylation by zDHHC17 in the Golgi membrane. S-palmitoylation of DGK ϵ by zDHHC7 likely proceeds analogously. All S-acyltransferases first bind a palmitic acid residue (red) in the DHHC domain and then transfer it to a cysteine residue in the substrate protein. zDHHC17 is unique in that it has six transmembrane helices, whereas most zDHHCs have four. It also has an ankyrin-repeat domain (ANK) at the N terminus involved in interactions with other proteins.

S-palmitoylated mDGK ϵ -Myc was also significant but lower—about 2.5-fold above the GST control. The amount of nonpalmitoylated mDGK ϵ -Myc also increased in these conditions (by about 40%), whereas the fraction of PEGylated mDGK ϵ -Myc accounted for 32% of the total protein (Fig. 5C, D). As expected, when the Cys38Ala mDGK ϵ -Myc was coexpressed with zDHHC7 instead of wild-type mDGK ϵ -Myc, no PEGylated (i.e., S-palmitoylated) form could be detected (Fig. 5B). In all samples, the mass shift of PEGylated mDGK ϵ -Myc corresponded to the binding of one PEG molecule per mDGK ϵ -Myc molecule, as confirmed by an analysis of flotillin-1 PEGylation (not shown), which is known to be S-palmitoylated at a single cysteine (50). However, under conditions favoring strong mDGK ϵ -Myc S-palmitoylation, such as its coexpression with zDHHC7, an additional faint band appeared above the main one, which could indicate a second site of S-palmitoylation (Fig. 5C).

To ensure that the above observations are not unique to the mDGK ϵ and are applicable to DGK ϵ of other

vertebrates as well, we assessed the S-palmitoylation of endogenous hDGK ϵ in HEK293 cells (Fig. 5E, F). Up to 23% of hDGK ϵ was PEGylated in cells not transfected with ectopic zDHHCs, resembling the percentage of modified mDGK ϵ -Myc in corresponding samples. Again, only one site of hDGK ϵ PEGylation was detected (Fig. 5F). The fraction of modified hDGK ϵ did not change in the presence of overexpressed zDHHC7, 17 or 6/16 (Fig. 5F), which suggests that endogenous zDHHC(s) S-palmitoylated the kinase to the maximal level.

S-palmitoylation inhibits DGK ϵ activity

The enzymatic activity of wild-type, Cys38Ala, and Pro31Ala forms of mDGK ϵ -Myc was determined using NBD-SAG-containing mixed micelles in HEK293 homogenates, detergent lysates, and mDGK ϵ -Myc immunoprecipitates, in conditions established earlier to ensure a linear dependence of NBD-SAPA production with respect to time and kinase content (19). The NBD-SAPA produced by DGK ϵ was separated by TLC and related to

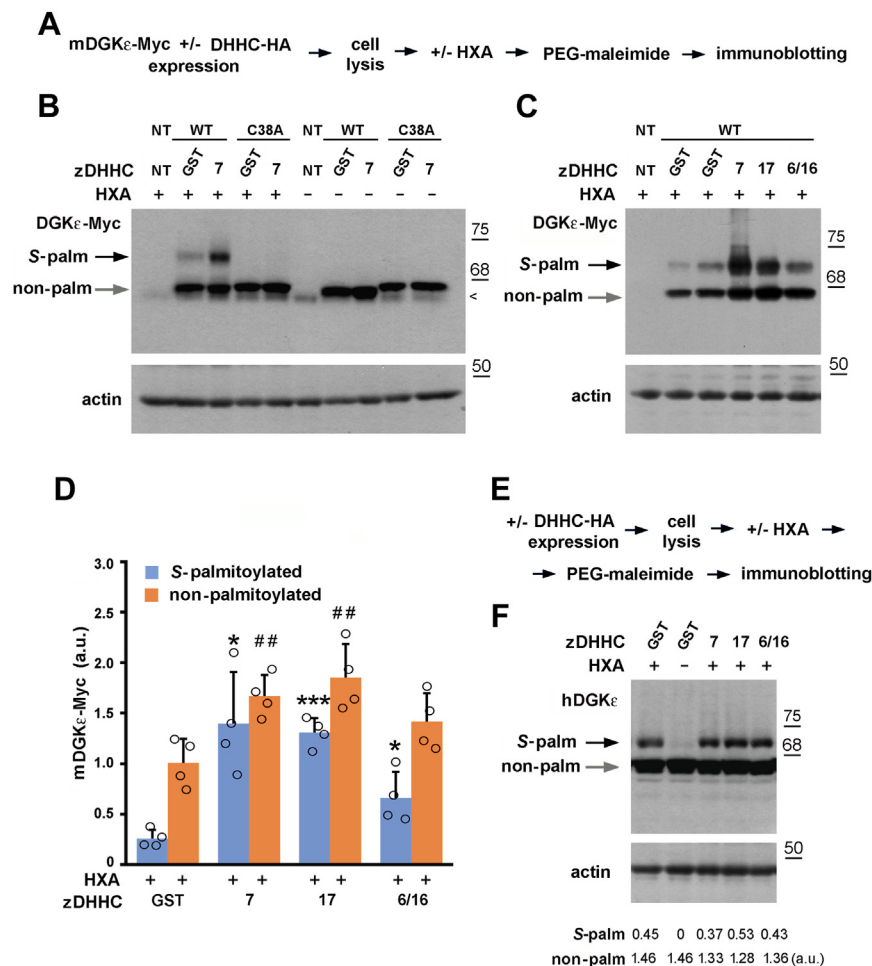


Fig. 5. zDHHC7, 17, and 6/16 S-palmitoylate DGK ϵ at one cysteine residue. A–D: HEK293 cells were transfected with plasmids encoding WT mDGK ϵ -Myc or Cys38Ala mDGK ϵ -Myc together with indicated zDHHC-HA or GST-HA in controls. After 24 h, cells were lysed and proteins were subjected to the APE procedure involving treatment with HXA (HXA+) or not (HXA–) and incubation with PEG-maleimide. A: Scheme of the APE procedure. B, C: mDGK ϵ -Myc (upper panels) and actin (lower panels) in cell lysates revealed with mouse anti-Myc and mouse anti-actin antibody, respectively. Arrowhead indicates a band recognized unspecifically by the anti-Myc antibody. D: The extent of DGK ϵ S-palmitoylation. The content of PEGylated (originally S-palmitoylated) and non-palmitoylated mDGK ϵ -Myc was determined by densitometry and normalized against actin. Data are mean \pm SD from four experiments. *, ***, significantly different at $P < 0.05$ and $P < 0.001$, respectively, from S-palmitoylated form in cells coexpressing mDGK ϵ -Myc and GST-HA; ##, significantly different at $P < 0.01$ from nonpalmitoylated form in cells coexpressing mDGK ϵ -Myc and GST-HA. E, F: HEK293 cells were transfected with plasmid encoding indicated zDHHC-HA or GST-HA in controls. After 24 h, cells were lysed and proteins were subjected to the APE procedure. E: Scheme of the APE procedure. F: Endogenous hDGK ϵ (upper panel) and actin (lower panel) in cell lysates revealed with sheep anti-DGK ϵ and mouse anti-actin antibody, respectively. Numbers below blots indicate amount of palmitoylated and nonpalmitoylated endogenous hDGK ϵ determined as in (D). Molecular weight markers in kDa are shown on the right. NT, cells not transfected.

the NBD-PDPA standard (Fig. 6A, D). In parallel, the content of the respective mDGK ϵ -Myc protein in the samples was quantified by immunoblotting using GST-hDGK ϵ as a standard (Fig. 6B, E). The specific activity of wild-type mDGK ϵ -Myc in homogenates was about 11 pmol SAPA/min/ng DGK ϵ at 1.45 mol% SAG and did not change when the latter was increased to 4.46 mol% (Fig. 6A–C). The Cys38Ala substitution increased the mDGK ϵ -Myc activity by about 20% at 1.45 mol% SAG and by a further 12% at 4.46 mol% SAG in comparison to the wild-type mDGK ϵ -Myc, yet the differences did not show the statistical significance (Fig. 6A–C). In contrast, the Pro31Ala substitution reduced the mDGK ϵ -Myc

activity significantly by 48% and 42% at 1.45 and 4.46 mol% SAG, respectively (Fig. 6A–C).

The results were reproduced when the activity of mDGK ϵ -Myc was measured at 1.45 mol% SAG in HEK293 lysates obtained with 1% NP-40. The activity of Cys38Ala mDGK ϵ -Myc was by about 30% (nonsignificantly) higher than the activity of wild-type mDGK ϵ -Myc (Fig. 6D, E, dark bars in 6F) and that of Pro31Ala mDGK ϵ -Myc activity lower by about 33% (significantly) (supplemental Fig. S5A, B, dark bar in supplemental Fig. S5C). Finally, we assessed the activity of the indicated forms of mDGK ϵ -Myc after their immunoprecipitation to minimize a potential influence of

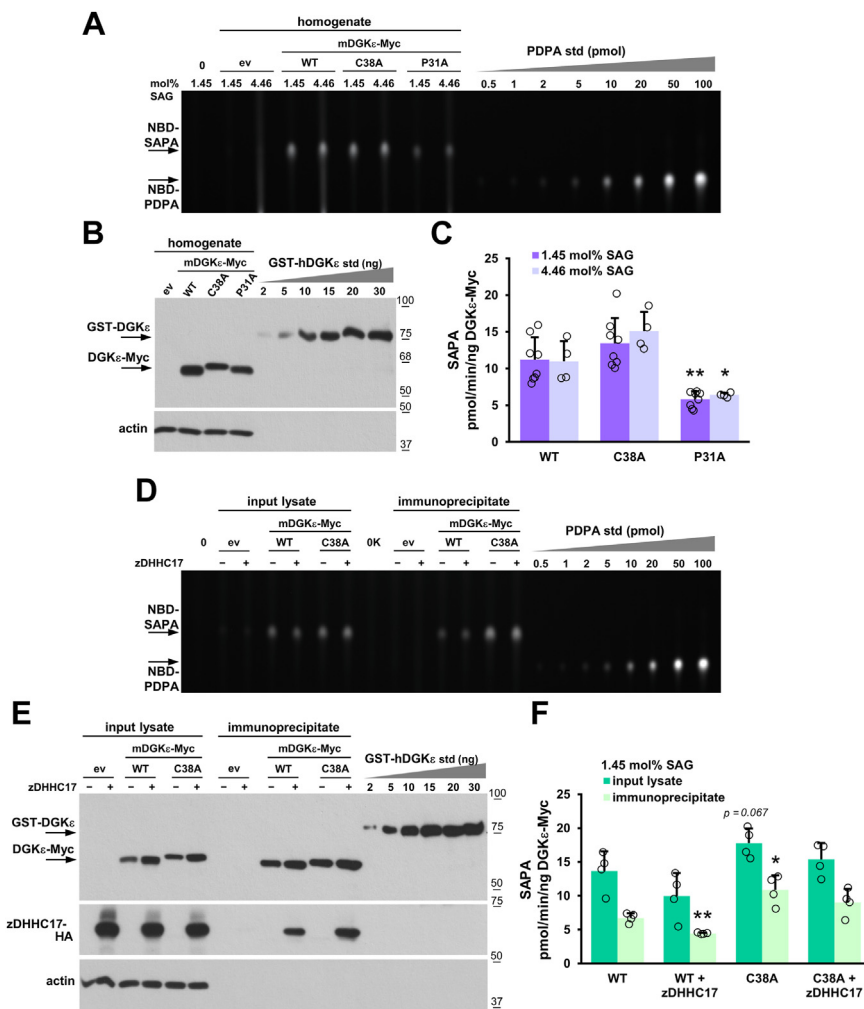


Fig. 6. *S*-palmitoylation inhibits DGK ϵ activity. HEK293 cells were transfected with indicated mDGK ϵ -Myc variants or with empty vector (ev) with or without zDHHC17-HA and either homogenized by sonication after 48 h or subjected to cell lysis after 24 h in 1% NP-40 with or without a following mDGK ϵ -Myc immunoprecipitation. The DGK ϵ activity was determined in cell homogenates (A–C) or lysates of mDGK ϵ -Myc-expressing cells (A) or in lysates of those cells and in the mDGK ϵ -Myc-immunoprecipitates (D). (0), samples devoid of cell homogenate or lysate, in (0K) supplemented with the Myc-Trap Agarose. Reactions were carried out using 15 μ g of total homogenate or lysate protein per sample or using mDGK ϵ -Myc immunoprecipitate obtained from 75 μ g of lysate protein. Lipids from 1/50 (A) or 1/10 (D) of the reaction mixture were separated by TLC. NBD-PDPA is used as a standard, it migrates more slowly on TLC than NBD-SAPA. B, E: Content of indicated overexpressed mDGK ϵ -Myc variants (upper panel) and actin (lower panel) in cell homogenates, lysates, and mDGK ϵ -Myc-immunoprecipitates revealed by immunoblotting with sheep anti-DGK ϵ and mouse anti-actin antibody, respectively. GST-hDGK ϵ is used as a standard. In (E) also zDHHC17-HA is revealed. Three micrograms of total homogenate protein (B) or 10 μ g of the total lysate protein or one-third of the mDGK ϵ -Myc immunoprecipitate (E) were applied per lane. C, F: Specific activity of indicated mDGK ϵ -Myc variants calculated after subtraction of the activity of endogenous DGKs determined in control cells (ev). Molecular weight markers in kDa are shown on the right. Data are mean \pm SD from eight (1.45 mol% SAG) or four (4.46 mol% SAG) experiments in (C) and from four experiments in (F). * and **, significantly different at $P < 0.05$ and $P < 0.01$, respectively, from samples of WT mDGK ϵ -Myc analyzed at corresponding mol% SAG. NBD-SAPA, 1-NBD-stearoyl-2-arachidonoyl-*sn*-glycero-3-phosphate.

unidentified factors present in cell homogenates and lysates. In these conditions, the specific activity of wild-type mDGK ϵ -Myc dropped to about 6 pmol SAPA/min/ng DGK ϵ , as found earlier (19). The activity of immunoprecipitated Cys38Ala mDGK ϵ -Myc was significantly higher, by as much as 62% relative to that of wild-type mDGK ϵ -Myc, which effect was likely underestimated as only about 20% of the wild-type mDGK ϵ -Myc was *S*-palmitoylated (Fig. 6D, E, light bars

in 6F). To circumvent this problem, we overproduced wild-type mDGK ϵ -Myc together with zDHHC17-HA at conditions inducing its hyperpalmitoylation (Fig. 5D). Under these conditions, the specific activity of mDGK ϵ -Myc was significantly lower, by 34% in comparison to wild-type mDGK ϵ -Myc overproduced without zDHHC17 (Fig. 6D, E, light bars in 6F). Taken together, the data indicate that *S*-palmitoylation of DGK ϵ at Cys38 reduces its enzymatic activity. As before, the Prol3Ala

mutation reduced the mDGK ϵ -Myc activity measured in its immunoprecipitate (supplemental Fig. S5A, B, light bars in supplemental Fig. S5C).

Rather unexpectedly, the activity of the non-palmitoylable Cys38Ala mDGK ϵ -Myc tended to decrease in the presence of zDHHCl7-HA (Fig. 6D, E, light bars in 6F). We observed that zDHHCl7-HA coimmunoprecipitated with both wild-type and Cys38Ala mDGK ϵ -Myc (Fig. 6E). These findings suggest that the interaction of zDHHCl7 with mDGK ϵ -Myc alone downregulates its activity even in the absence of S-palmitoylation, whereas the S-palmitoylation of mDGK ϵ -Myc reduces it further.

mDGK ϵ -Myc is localized in the endoplasmic reticulum and in small amounts in the Golgi apparatus

To analyze the cellular localization of mDGK ϵ -Myc overproduced in HEK293 cells, we applied confocal microscopy and markers of the endoplasmic reticulum and the Golgi apparatus. STIM1 was used as a marker of the endoplasmic reticulum membranes and GM130 and golgin-97 as markers of Golgi membranes (38, 51). To quantitate the distribution of mDGK ϵ -Myc, optical sections of triple-labeled cells (including nucleus labeling) were used to reconstruct 3D images of the mDGK ϵ -Myc-, STIM1-, GM130-, or golgin-97-decorated structures (ROI). Next, Manders' colocalization coefficients were calculated for mDGK ϵ -Myc and each of the marker proteins in the respective ROI. This coefficient scores colocalization regardless of the linear relationship between the intensity of the two signals (39). It allowed us to determine the fraction of a cellular organelle (ROI) decorated by a given marker protein overlapping a DGK ϵ -Myc-positive region (M1) and vice versa (M2). As could be expected from earlier studies (47, 48), mDGK ϵ -Myc was abundant in the STIM1-decorated endoplasmic reticulum yielding a white pattern in merged images (Fig. 7A1–C1 and supplemental Fig. S6A1–C1). The image analysis (Fig. 7D1, supplemental Fig. S6D1 and supplemental Video S1) revealed that as much as 80–90% of the STIM1-decorated ROI overlapped with the DGK ϵ -Myc-decorated ROI (Table 1, M1) and 50–60% of DGK ϵ -Myc-positive ROI colocalized with STIM1-positive ROI (Table 1, M2). STIM1 was concentrated in the perinuclear region resembling the pattern observed earlier in resting HEK293 cells (52). DGK ϵ -Myc and STIM1 colocalized to a high extent in this perinuclear part of the endoplasmic reticulum while they tended to be separated toward the cell periphery (Fig. 7C1 and supplemental Fig. S6C1). This “separate” fraction of DGK ϵ -Myc could be located either in the endoplasmic reticulum devoid of STIM1 or in some other cellular compartment(s).

In order to examine the localization of mDGK ϵ -Myc in the Golgi apparatus, suggested by its zDHHCl7- and zDHHCl7-catalyzed S-palmitoylation, we utilized a protocol optimized for Golgi staining, which relies on the cell permeabilization with digitonin at room

temperature (38) and used GM130 as a *cis*-Golgi marker (Fig. 7A2–D2, supplemental Fig. S6A2–D2 and supplemental Video S2) and golgin-97 as a *trans*-Golgi marker (Fig. 7A3–D3, supplemental Fig. S6A3–D3 and supplemental Video S3). With this approach, we revealed the presence of some mDGK ϵ -Myc in the Golgi apparatus seen as white spots of its colocalization with GM130 or golgin-97 in Fig. 7C2 and C3 and supplemental Fig. S6C2, C3. The white spots can also be observed on merged images of four sequential optical sections shown in Fig. 7C2'–C2''' for mDGK ϵ -Myc and GM130 and in Fig. 7C3'–C3''' for mDGK ϵ -Myc and golgin-97. However, for most regions, the intensities of the mDGK ϵ -Myc and GM130 or golgin-97 signals were different from each other not allowing the signals to converge to white. Subsequent image analysis indicated that the fraction of mDGK ϵ -Myc-positive ROI that colocalized with the GM130-positive or golgin-97-positive ROI reached 3–3.5% (Table 1, M2), whereas as much as 70–90% of either GM130- or golgin-97-decorated Golgi overlapped the mDGK ϵ -Myc-decorated ROI (Table 1, M1). These data indicated that only a small fraction of the total cellular mDGK ϵ -Myc was located in the Golgi apparatus and was distributed through the whole compartment.

We performed a series of control experiments to verify the specificity of the analyzed signals, including the detection of the marker proteins in the absence of the anti-Myc antibody and vice versa. No unexpected signal was detected in these conditions (supplemental Fig. S7 and data not shown) ruling out the possibility of fluorescence bleeding.

DISCUSSION

The DGK family comprises 10 isoenzymes catalyzing phosphorylation of DAG; their activity is likely fine-tuned by cotranslational/post-translational modifications. To date, however, the data on mDGK ϵ /hDGK ϵ modifications are limited to its ubiquitination at Lys354/357, a scarcity of information surprising in view of the detailed data on the allosteric regulation of DGK ϵ activity found with purified hDGK ϵ (20). Cotranslational/post-translational modifications of all other DGKs are also poorly known, with the exception of their phosphorylation (53). Our earlier study indicated that DGK ϵ can undergo palmitoylation, as revealed by global palmitoylome analysis in Raw264 macrophage-like cells, when also an increase in the amount of palmitoylated mDGK ϵ was detected in cells stimulated with lipopolysaccharide (29). In the present work, we showed that m/hDGK ϵ is S-palmitoylated at Cys38/40 and investigated various aspects of this modification in some detail.

Cys38/40 is located at the cytoplasmic side of a putative membrane-bound α -helix of mDGK ϵ /hDGK ϵ adopting either a transmembrane topology or a

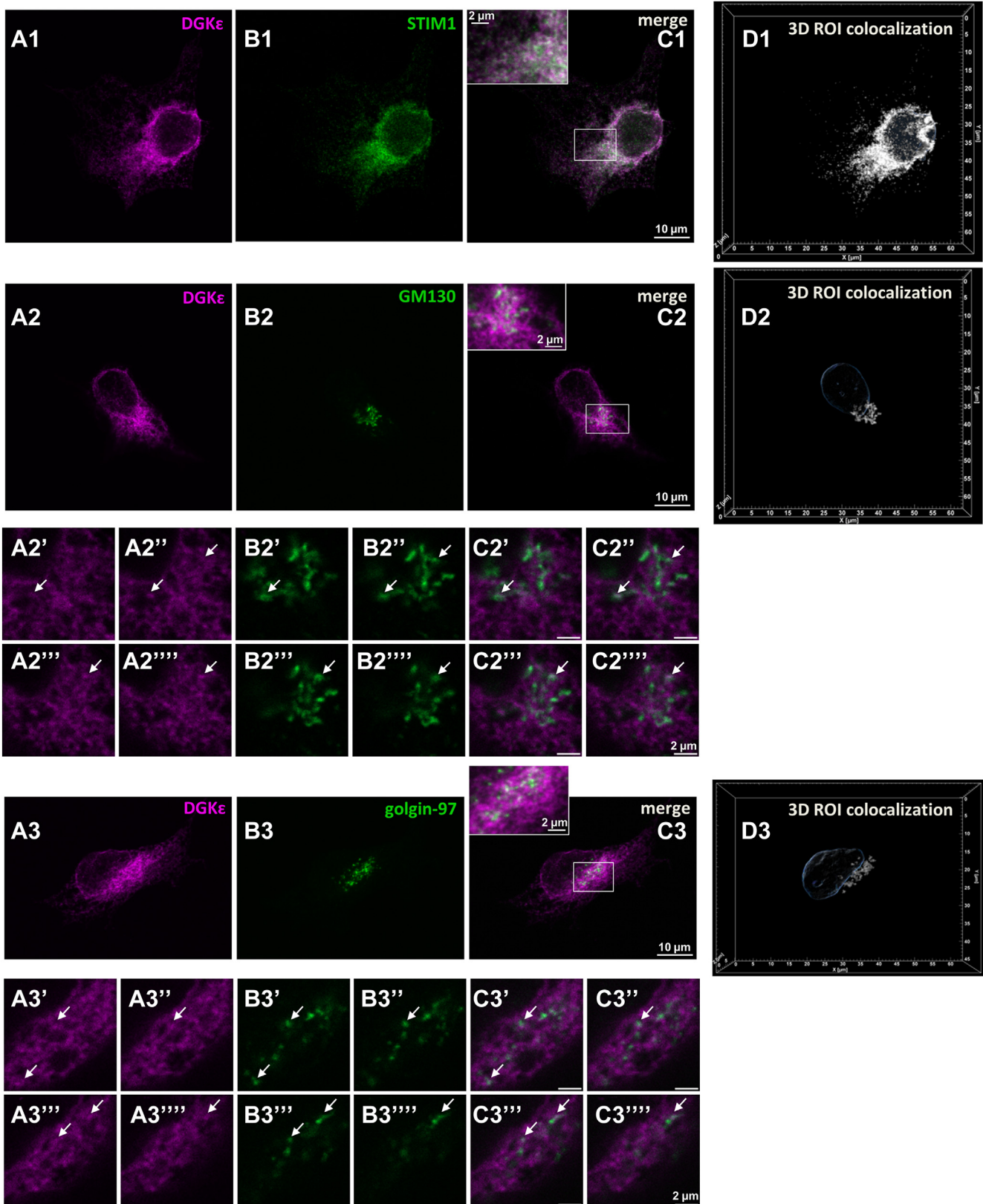


Fig. 7. mDGK ϵ -Myc is localized to the endoplasmic reticulum and to the Golgi apparatus. HEK293 cells were transfected with mDGK ϵ -Myc, and after 48 h, cells were fixed with 4% paraformaldehyde and permeabilized with 0.05% Triton X-100 (for endoplasmic reticulum staining) or with 0.005% digitonin (for Golgi staining). A1–A3: Localization of mDGK ϵ -Myc, (B1) STIM1, (B2) GM130, (B3) golgin-97. C1–C3: Merged images of mDGK ϵ -Myc and the respective marker protein. Colocalized mDGK ϵ -Myc and marker protein appear white. z-Stack images of 10 optical sections taken in the middle of a cell are shown. Insets in (C1–C3) show enlarged images of marked fragments. (A2'–A2''''') Four consecutive optical sections through the Golgi showing mDGK ϵ -Myc, (B2'–B2''''') GM-130, and (C2'–C2''''') merged image. (A3'–A3''''') Four consecutive optical sections through the Golgi showing

TABLE 1. Subcellular distribution of mDGKε-Myc

Marker protein	Experiment	M1 (%)	M2 (%)	<i>n</i>
STIMI	I	90.0 ± 12.4	62.6 ± 19.4	13
(endoplasmic reticulum)	II	81.6 ± 16.1	49.7 ± 12.0	13
GMI30	I	78.4 ± 18.6	3.6 ± 1.5	14
(<i>cis</i> -Golgi)	II	92.2 ± 8.4	2.9 ± 1.2	13
Golgin-97	I	94.2 ± 9.9	3.3 ± 1.4	16
(<i>trans</i> -Golgi)	II	89.3 ± 11.2	1.2 ± 0.5	21

M1, percentage of STIMI, GMI30, and golgin-97-positive ROI overlapping mDGKε-Myc-positive ROI; M2, percentage of mDGKε-Myc-positive ROI overlapping STIMI, GMI30, and golgin-97-positive ROI.

HEK293 cells were transfected and stained as described in Fig. 7. Data are mean ± SD. *n* = number of cells analyzed.

U-shaped intramembrane one with Pro31/33 serving as hinge (9). It has been estimated that in about 95% of single-pass integral membrane proteins, their palmitoylation site is located either at a juxtamembrane or an intramembrane cysteine (54), and DGKε fits the first model. Notably, the intramembrane Cys26 of mDGKε was shown here not to be modified. Cys38 is by far the predominant site of DGKε S-palmitoylation but perhaps not the only one, as the Cys38Ala substitution eliminated about 93% of the modification detected with click and ABE but not all of it. The site(s) of this residual S-palmitoylation has neither been determined nor is it known whether it even occurs in native DGKε. Our preliminary mass spectrometry analyses argue against such a possibility (not shown). There are as many as 28 cysteines in mDGKε/hDGKε. So far, no consensus sequence for protein S-acylation has been defined conclusively, but Cys72, 73, 75, 87, 88, 149, and 417 of mDGKε (and corresponding Cys residues in hDGKε) are predicted by the SwissPalm database to undergo S-palmitoylation with high or medium confidence (<https://swissplam.org>, October 20, 2023). Notably, all those cysteines except for the latter one are localized to the cysteine-rich domains C1A (amino acids 58/60–106/108 in m/hDGKε) and C1B (amino acids 122/125–174/177) of DGKε. We have found recently that selected cysteine and histidine residues of the C1B domain of mDGKε form a zinc-finger motif controlling the activity of the kinase and its proteasomal degradation (19). Notably, Cys72/74 and 75/77 belong to an incomplete zinc finger motif lacking a His residue in the C1A domain, whereas Cys73/75, Cys87/89, and Cys 149/152 are not part of the respective motif in C1A and C1B domains (Fig. 5 in Ref. (19)), potentially being available for S-acylation. A global proteomic analysis of

S-acylated sites in proteins of the mouse forebrain indicated that Cys132 and Cys135 of the mDGKε C1B domain are modified (39), whereas our study excluded it. With all the above in mind, we tend to believe that some cysteine residue(s) of the C1A and C1B domains of DGKε can be prone to unspecific labeling at an excess of 17ODYA during metabolic labeling of cells (click technique) and are also not fully reduced/blocked during the ABE procedure, allowing their subsequent biotinylation and false-positive detection.

We identified zDHHC7, zDHHC17, and zDHHC6/16 as candidate mDGKε S-acyltransferases using the so-called “Fukata screen” (26, 35) followed by ABE and APE assays. zDHHC7 and zDHHC17 were more effective than zDHHC6/16 in the model studies. The extent of DGKε S-palmitoylation by zDHHC7 or zDHHC17 increased profoundly when the amounts of plasmids encoding these proteins used for transfection were doubled. These results confirm the obvious supposition that the contribution of a particular isoenzyme to the *in vivo* modification of endogenous DGKε would be strongly affected by the possibility of their encounter. The identified zDHHCs differ substantially in their cellular localization, enzymatic activity, and also preferences for the acyl-CoA species. zDHHC6 is found exclusively in the endoplasmic reticulum where also DGKε is unequivocally localized, as indicated by the colocalization of mDGKε-Myc with STIMI in this study and by earlier data obtained for overproduced DGKε as well (47, 48). zDHHC6 catalyzes S-palmitoylation of crucial local proteins under the control of zDHHC16, which S-palmitoylates zDHHC6 potentially at three cysteine residues of its C-terminal region, with non-palmitoylated zDHHC6 being inactive. The two major S-palmitoylated forms of zDHHC6 are, respectively, highly active but short lived and moderately active but more stable, pointing to a tight regulation of zDHHC6 functioning (49) which was also reflected by a very low level of zDHHC6 overexpression in our studies. On the other hand, zDHHC7 and zDHHC17 reside in the Golgi apparatus, as indicated by studies on human and mouse zDHHCs overexpressed in HEK293 and HeLa cells (25, 27). zDHHC7 has a high S-acyltransferase activity potentially toward multiple substrate proteins and prefers C14/C16 over C18 acyl-CoA. zDHHC17, with a weaker enzymatic activity, utilizes preferentially the longer C16/C18 rather than C14 acyl-CoA species (55–57). We found that a small fraction of mDGKε-Myc was located in the Golgi apparatus, which could enable its S-palmitoylation by zDHHC7 and zDHHC17. We

mDGKε-Myc, (B3'–B3''') golgin-97, and (C3'–C3''') merged images. Arrows point to Golgi fragments with intensive staining of both mDGKε-Myc and the respective marker protein. D1–D3: Reconstructed 3D images of two colocalized ROI positive for mDGKε-Myc and STIMI (D1) or GMI30 (D2) or golgin-97 (D3). Contours of the nucleus detected by Hoechst 33342 staining are shown in blue. ROI as these were used for quantitative analysis of mDGKε-Myc distribution presented in Table 1. mDGKε-Myc (magenta) was visualized with mouse anti-Myc IgG followed by donkey anti-mouse IgG-Alexa647. STIMI, GMI30, and golgin-97 (green) were visualized with rabbit anti-STIMI, anti-GMI30, and anti-golgin-97 IgG followed by donkey anti-rabbit IgG-FITC. Additional cells stained according to this protocol are shown in supplemental Fig. S6.

achieved this by using a cell staining protocol preserving the Golgi structure (38) followed by quantitative image analysis. The specificity of the staining procedure and the small amount of mDGK ϵ -Myc found in the Golgi explain the lack of such observations in earlier studies on the cellular location of DGK ϵ . One should bear in mind that the overexpression of zDHHCl7 and mDGK ϵ could affect their cellular localization, and that 17ODYA used by us for metabolic labeling did not allow discriminating between C16 and C18 acyl chain as natural DGK ϵ S-acylation substrates. All the above features are not sufficient to indicate which S-acyltransferase isoenzyme is responsible for the DGK ϵ acylation in native conditions. It is of interest in this context that mDGK ϵ /hDGK ϵ carries the QP motif found in some zDHHCl7 substrates allowing their recognition and binding by the ankyrin-repeat domain of the S-acyltransferase (57, 58). zDHHCl7 coimmunoprecipitated with mDGK ϵ -Myc in our studies, suggesting, although not proving (59) that DGK ϵ could be a natural target of S-acylation by zDHHCl7.

The detection of DGK ϵ S-palmitoylation, which in HEK293 cells affects about one in four molecules of endogenous hDGK ϵ , raises the question of its physiological significance. Our data indicate that S-palmitoylation inhibits the DGK ϵ activity and promotes its accumulation in cells. DGK ϵ has a putative N-terminal transmembrane or re-entrant α -helix, and the effects of the S-palmitoylation at the cysteine located in the cytoplasmic end of the α -helix can be analogous to those observed for LRP6 or calnexin, both transmembrane proteins of the endoplasmic reticulum S-palmitoylated at juxtamembrane cysteines. S-palmitoylation of LRP6 (a protein involved in Wnt signaling) is postulated to induce tilting of its transmembrane fragment, thereby enabling an adjustment of its effective length to the thickness of the endoplasmic reticulum membrane (60). It also cooperates with monoubiquitination to prevent proteasomal degradation of LRP6 (41). A similar mechanism can explain the observed accumulation of S-palmitoylated DGK ϵ and hyperpalmitoylation of Cys135Ala mDGK ϵ -Myc that is avidly degraded by the 26S proteasome (19). The consequences of the S-palmitoylation for the conformation of calnexin, an endoplasmic reticulum chaperone that promotes the folding of glycoproteins, are even more complex. The transmembrane fragment of calnexin is also predicted to be tilted in the membrane. Interestingly, the calnexin α -helix is additionally kinked because of the presence of a proline residue somewhat similar to Pro31/33 of mDGK ϵ /hDGK ϵ . The S-palmitoylation of calnexin by zDHHCl6 does affect neither the proline-induced kink nor the α -helix tilt in the membrane. However, it is predicted to affect the orientation of its cytosolic fragment with respect to the α -helix axis and can favor the partitioning of calnexin to sheet-like perinuclear structures of the endoplasmic reticulum. As a result, calnexin is properly positioned to capture its client proteins (24).

A recent prediction of hDGK ϵ structure indicates that its N-terminal fragment is tilted in the membrane and its conformation determines the distance between the active site and the SAG-bearing membrane. It is proposed that shortening of the distance, facilitating the kinase enzymatic activity, occurs as a result of bending of the transmembrane fragment at Pro33, and such conformational changes can be prevented by the interaction of the positively charged N-terminal amino acids of DGK ϵ with PS in the membrane (4). It seems possible that S-palmitoylation of Cys38/40 cooperates with Pro31/33 in a similar manner, preventing the conformational changes of its transmembrane helix and thereby inhibiting DGK ϵ activity. Our data, obtained using immunoprecipitated mDGK ϵ -Myc, are consistent with an earlier finding that the whole N-terminal 50-amino acid-long fragment of hDGK ϵ comprising the transmembrane fragment and the following cluster of positively charged amino acids inhibits the kinase activity, as was determined using an N-terminally truncated purified hDGK ϵ (4). Of note, we found that zDHHCl7 coimmunoprecipitated with mDGK ϵ -Myc, including its Cys38A mutant form, and tended to downregulate (yet insignificantly) the activity of the mutant form of mDGK ϵ -Myc. In this case, the significant inhibition of the wild-type mDGK ϵ -Myc activity found in the presence of zDHHCl7 can in fact result from a synergy of the zDHHCl7 binding DGK ϵ and its S-palmitoylation. In addition, the interaction of DGK ϵ with zDHHCl7 can increase the cellular abundance of the kinase, and this effect was observed in some experiments even for the Cys38Ala mDGK ϵ -Myc mutant form (Fig. 6).

Our study also shows that the Pro31Ala mutation reduces DGK ϵ activity markedly, in agreement with earlier studies (3). In light of the model discussed above, this inhibition may result from hindering the conformational change of the DGK ϵ N terminus required for its activation. However, in our hands, the Pro31Ala mutation also enhanced the protein degradation in a reproducible manner. We have recently found that certain mDGK ϵ mutants, especially those in its CIB zinc finger, are inactive, likely misfolded, and degraded by the 26S proteasome (19). The Pro31Ala substitution could have a global effect on DGK ϵ folding (hence stability), thereby reducing its enzymatic activity. We base this assumption on the fact that the N-terminally truncated hDGK ϵ had a higher activity but formed insoluble precipitates unless tagged at the N terminus with His-SUMO (4), indicating an involvement of this DGK ϵ fragment in maintaining proper protein conformation.

Our present study suggests that the S-palmitoylation of DGK ϵ can affect its cellular transport and localization. Owing to its strict specificity toward SAG, DGK ϵ has been proposed to contribute to the PI cycle, which serves to rebuild PI(4,5)P₂ level after its hydrolysis triggered by a number of plasma membrane receptors

(9, 17). The cycle operates at the plasma membrane-endoplasmic reticulum contact sites formed by STIM1-Orail proteins during the receptor activation and requires an involvement of proteins transporting lipids between these two membranes. A discovery of extended synaptotagmins, which mediate bidirectional transport of glycerophospholipids and DAG, suggests that the PA of the PI cycle can be formed by DGK ϵ in the endoplasmic reticulum (61). On the other hand, the Nir2 protein transports PA from the plasma membrane toward the endoplasmic reticulum in exchange for PI traveling in the opposite direction, thus placing the SAG to PA phosphorylation in the plasma membrane (62, 63). Taking into account that DGK ϵ can be S-palmitoylated by zDHHC7 and zDHHC17, one can speculate that it undergoes this modification during its anterograde vesicular trafficking toward the plasma membrane to be kept inactive until its depalmitoylation. S-palmitoylation at the cytoplasmic end of transmembrane fragments has recently been identified as a signal guiding diverse transmembrane proteins to the cisternal rims of the Golgi because of its impact on the shape of the transmembrane fragment (its conversion toward a cone-like one). Thanks to such sorting, the acylated proteins are efficiently transported through the Golgi stacks to the plasma membrane (25), and similar trafficking of DGK ϵ S-palmitoylated by zDHHC7 or zDHHC17 can be envisioned. A fraction of overexpressed DGK ϵ was localized in the plasma membrane by earlier observations (3), although in our hands mDGK ϵ -Myc was hardly found in this location (unpublished data).


DGK ϵ contributes to lipid metabolism preventing obesity, an activity attributed to DGK ϵ located in the endoplasmic reticulum (13, 64). Furthermore, there are data that question the possibility that DGK ϵ is the sole kinase capable of producing PA required in the PI cycle. Silencing of DGK ϵ alone did not affect the angiotensin-induced PI resynthesis, clearly pointing to an involvement of other DGKs. On the other hand, the PI resynthesis was inhibited strongly by the DGK inhibitor R59022 (10) affecting DGK ϵ , α , and θ only (65). It has also been found that siRNA silencing of DGK ϵ , and also of DGK α , δ , η , ζ , or θ , alone did not diminish the 38:4 PA and PI synthesis in unstimulated HEK293 cells (66). To sum up, those two studies indicate that the activity of DGKs other than DGK ϵ , some selective to distinct DAG species (8), is important for the synthesis of PI and its phosphorylated derivatives both in resting cells and during their activation followed by PI(4,5)P $_2$ hydrolysis. We found that a stable downregulation of DGK ϵ using shRNA in resting Raw264 cells decreased the phosphorylation of 38:4 DAG (SAG) to PA by 40% (19), a downregulation quite substantial vis-à-vis the reported lack of an effect of DGK ϵ silencing on PI synthesis found in HEK293 cells. Taken together, the data indicate that, in the absence of DGK ϵ , other DGKs can substitute for its function in de novo synthesis and resynthesis of the major pool of PA/PI.

On the other hand, our data indicating the localization of a small fraction of DGK ϵ in the Golgi apparatus allow us to speculate about its engagement in the maintenance of the local pool of PI(4)P. It has been shown that PI(4)P can be transported from the Golgi toward the plasma membrane (67) and can also be hydrolyzed by most phospholipase C isoforms (68). The PI(4)P-derived SAG lasts longer than the SAG produced by PI(4,5)P $_2$ hydrolysis, the major function of which would then be the generation of the IP $_3$ -mediated Ca $^{+2}$ signal. Furthermore, the phospholipase C-dependent hydrolysis of PI(4)P at the Golgi is required for the DAG-mediated activation of nuclear PKD during cardiac hypertrophy (68) placing DGK ϵ as a potential terminator of that signal concomitant with the resynthesis of the local pool of PA/PI(4)P. The DGK ϵ S-palmitoylation in the Golgi can facilitate its local retention and increase its abundance, keeping the kinase ready for activation upon depalmitoylation.

Limitations

The results presented in this study were obtained using mDGK ϵ -Myc overproduced in HEK293 cells. This approach does not undermine the robustness of the detection of the S-palmitoylation of mDGK ϵ /hDGK ϵ on Cys38/40 or its negative influence on the DGK ϵ activity, although further studies are required to quantitate the kinetic parameters of purified Cys38Ala mDGK ϵ -Myc. Furthermore, the physiological extent of the S-palmitoylation of endogenous DGK ϵ by ZDHHC6/16, 7, and 17 can be properly evaluated only by studies of DGK ϵ and the indicated zDHHCs expressed at their native levels. The overexpression of DGK ϵ can in fact result in an underestimation of its Golgi pool. Studies of native DGK ϵ can verify the intriguing possibility of the DGK ϵ involvement in the SAG circulation in the Golgi apparatus, which has not been considered so far.

Data availability

The data that support findings of this study are available from the corresponding author on request. 

Supplemental data

This article contains [supplemental data](#).

Acknowledgments

The authors thank Prof Masaki Fukata from the National Institute of Physiological Sciences in Okazaki, Japan for the library of vectors bearing 1-23 DHHC Sacyltransferases. They also thank Dr Jan Fronk (retired), formerly at the Faculty of Biology, University of Warsaw for helpful comments, and Dr Orest V. Matveichuk from our Laboratory for a preliminary study on the identification of zDHHC modifying DGK ϵ . Confocal imaging was performed at the Laboratory of Imaging Tissue Structure and Function, a core facility at the Nencki Institute of Experimental Biology and a part of the infrastructure of the Polish Euro-BioImaging Node.

Author contributions

K. K. and G. T. conceptualization; G. T., A. H.-J., A. Ś., and A. C. formal analysis; G. T., A. H.-J., A. Ś., J. W., and A. C. investigation; K. K. writing—original draft; G. T., A. H.-J., A. Ś., J. W., A. C., and K. K. writing—review & editing; K. K. supervision; K. K. project administration; K. K. funding acquisition.


Author ORCIDiDs

Gabriela Traczyk  <https://orcid.org/0000-0003-2065-440X>
Aneta Hromada-Judycka  <https://orcid.org/0000-0002-4449-882X>

Anna Świątkowska  <https://orcid.org/0000-0003-1000-7882>

Julia Wiśniewska  <https://orcid.org/0000-0002-8541-6480>

Anna Ciesielska  <https://orcid.org/0000-0001-9902-494X>

Katarzyna Kwiatkowska  <https://orcid.org/0000-0002-0550-8394>

Funding and additional information

This work was supported by the National Science Centre, Poland (grant number: 2018/29/B/NZ3/00407). This work was also supported by a project financed by the Ministry of Education and Science based on contract no. 2022/WK/05 (Polish Euro-BioImaging Node “Advanced Light Microscopy Node, Poland”).

Conflict of interest

The authors declare that they have no conflicts of interest with the contents of this article.

Abbreviations

ABE, acyl-biotin exchange; aHUS, atypical hemolytic uremic syndrome; APE, acyl-PEG exchange; CI, cysteine-rich conserved homology-I; DAG, diacylglycerol; DGK ϵ , diacylglycerol kinase- ϵ ; GST, glutathione-S-transferase; HA, hemagglutinin; hDGK ϵ , human DGK ϵ ; HEK293, human embryonic kidney 293 cell line; HXA, hydroxylamine; mDGK ϵ , mouse DGK ϵ ; NBD-SAPA, 1-NBD-stearoyl-2-arachidonoyl-*sn*-glycero-3-phosphate; NBD-PDPA, 1-palmitoyl-2-NBD-dodecanoyl-*sn*-glycero-3-phosphate; NBD-SAG, 1-NBD-stearoyl-2-arachidonoyl-*sn*-glycero-3-phosphate; 17ODYA, 17-octadecynoic acid; PA, phosphatidic acid; PI, phosphatidylinositol; PS, phosphoserine; ROI, region of interest; SAG, C18:0/20:4 DAG; TCEP, Tris(2-carboxyethyl)phosphine hydrochloride; zDHHC, zinc finger DHHC domain containing.

Manuscript received March 30, 2023, and in revised form November 17, 2023. Published, JLR Papers in Press, November 24, 2023, <https://doi.org/10.1016/j.jlr.2023.100480>

REFERENCES

1. Sakane, F., Imai, S., Kai, M., Yasuda, S., and Kanoh, H. (2007) Diacylglycerol kinases: why so many of them? *Biochim. Biophys. Acta.* **1771**, 793–806
2. Franks, C. E., Campbell, S. T., Purow, B. W., Harris, T. E., and Hsu, K. L. (2017) The ligand binding landscape of diacylglycerol kinases. *Cell Chem. Biol.* **24**, 870–880.e5
3. Decaffmeyer, M., Shulga, Y. V., Dicu, A. O., Thomas, A., Truant, R., Topham, M. K., et al. (2008) Determination of the topology of the hydrophobic segment of mammalian diacylglycerol kinase ϵ in a cell membrane and its relationship to predictions from modeling. *J. Mol. Biol.* **383**, 797–809
4. Bozelli, J. C., Jr., Yune, J., Aulakh, S. S., Cao, Z., Fernandes, A., Seitova, A., et al. (2022) Human diacylglycerol kinase ϵ N-terminal segment regulates the phosphatidylinositol cycle, controlling the rate but not the acyl chain composition of its lipid intermediates. *ACS Chem. Biol.* **17**, 2495–2506
5. Tang, W., Bunting, M., Zimmerman, G. A., McIntyre, T. M., and Prescott, S. M. (1996) Molecular cloning of a novel human diacylglycerol kinase highly selective for arachidonate-containing substrates. *J. Biol. Chem.* **271**, 10237–10241
6. Pettitt, T. R., and Wakelam, M. J. (1999) Diacylglycerol kinase ϵ , but not ζ , selectively removes polyunsaturated diacylglycerol, inducing altered protein kinase C distribution in vivo. *J. Biol. Chem.* **274**, 36181–36186
7. Lung, M., Shulga, Y. V., Ivanova, P. T., Myers, D. S., Milne, S. B., Brown, H. A., et al. (2009) Diacylglycerol kinase ϵ is selective for both acyl chains of phosphatidic acid or diacylglycerol. *J. Biol. Chem.* **284**, 31062–31073
8. Ware, T. B., Franks, C. E., Granade, M. E., Zhang, M., Kim, K. B., Park, K. S., et al. (2020) Reprogramming fatty acyl specificity of lipid kinases via CI domain engineering. *Nat. Chem. Biol.* **16**, 170–178
9. Epand, R. M., So, V., Jennings, W., Khadka, B., Gupta, R. S., and Lemaire, M. (2016) Diacylglycerol kinase- ϵ : properties and biological roles. *Front. Cell Dev. Biol.* **4**, 112
10. Kim, Y. J., Sengupta, N., Sohn, M., Mandal, A., Pemberton, J. G., Choi, U., et al. (2022) Metabolic routing maintains the unique fatty acid composition of phosphoinositides. *EMBO Rep.* **23**, e54532
11. Rodriguez de Turco, E. B., Tang, W., Topham, M. K., Sakane, F., Marcheselli, V. L., Chen, C., et al. (2001) Diacylglycerol kinase ϵ regulates seizure susceptibility and long-term potentiation through arachidonoyl-inositol lipid signaling. *Proc. Natl. Acad. Sci. U. S. A.* **98**, 4740–4745
12. Zhang, N., Li, B., Al-Ramahi, I., Cong, X., Held, J. M., Kim, E., et al. (2012) Inhibition of lipid signaling enzyme diacylglycerol kinase ϵ attenuates mutant huntingtin toxicity. *J. Biol. Chem.* **287**, 21204–21213
13. Nakano, T., Seino, K., Wakabayashi, I., Stafforini, D. M., Topham, M. K., and Goto, K. (2018) Deletion of diacylglycerol kinase ϵ confers susceptibility to obesity via reduced lipolytic activity in murine adipocytes. *FASEB J.* **32**, 4121–4131
14. Lemaire, M., Frémeaux-Bacchi, V., Schaefer, F., Choi, M., Tang, W. H., Le Quintrec, M., et al. (2013) Recessive mutations in DGK ϵ cause atypical hemolytic-uremic syndrome. *Nat. Genet.* **45**, 531–536
15. Liu, D., Ding, Q., Dai, D. F., Padhy, B., Nayak, M. K., Li, C., et al. (2021) Loss of diacylglycerol kinase ϵ causes thrombotic microangiopathy by impairing endothelial VEGFA signaling. *JCI Insight.* **6**, e146959
16. Shindo, M., Irie, K., Masuda, A., Ohigashi, H., Shirai, Y., Miyasaka, K., et al. (2003) Synthesis and phorbol ester binding of the cysteine-rich domains of diacylglycerol kinase (DGK) isozymes. DGK γ and DGK β are new targets of tumor-promoting phorbol esters. *J. Biol. Chem.* **278**, 18448–18454
17. Shulga, Y. V., Topham, M. K., and Epand, R. M. (2011) Study of arachidonoyl specificity in two enzymes of the PI cycle. *J. Mol. Biol.* **409**, 101–112
18. Aulakh, S. S., Bozelli, J. C., Jr., and Epand, R. M. (2022) Exploring the alpha fold predicted conformational properties of human diacylglycerol kinases. *J. Phys. Chem. B.* **126**, 7172–7183
19. Traczyk, G., Świątkowska, A., Hromada-Judycka, A., Janikiewicz, J., and Kwiatkowska, K. (2022) An intact zinc finger motif of the CI domain is critical for stability and activity of diacylglycerol kinase- ϵ . *Int. J. Biochem. Cell Biol.* **152**, 106295
20. Bozelli, J. C., Jr., Jennings, W., Black, S., Hou, Y. H., Lemaire, D., Chatha, P., et al. (2018) Membrane curvature allosterically regulates the phosphatidylinositol cycle, controlling its rate and acyl-chain composition of its lipid intermediates. *J. Biol. Chem.* **293**, 17780–17791
21. Barylko, B., Mao, Y. S., Wlodarski, P., Jung, G., Binns, D. D., Sun, H.-Q., et al. (2009) Palmitoylation controls the catalytic activity and subcellular distribution of phosphatidylinositol 4-kinase II α . *J. Biol. Chem.* **284**, 9994–10003
22. Levental, I., Lingwood, D., Grzybek, M., Coskun, U., and Simons, K. (2010) Palmitoylation regulates raft affinity for the majority of integral raft proteins. *Proc. Natl. Acad. Sci. U. S. A.* **107**, 22050–22054

23. Stepanek, O., Draber, P., and Horejsi, V. (2014) Palmitoylated transmembrane adaptor proteins in leukocyte signaling. *Cell Signal.* **26**, 895–902
24. Lakkaraju, A. K., Abrami, L., Lemmin, T., Blaskovic, S., Kunz, B., Kihara, A., *et al.* (2012) Palmitoylated calnexin is a key component of the ribosome-translocon complex. *EMBO J.* **31**, 1823–1835
25. Ernst, A. M., Syed, S. A., Zaki, O., Bottanelli, F., Zheng, H., Hacke, M., *et al.* (2018) S-Palmitoylation sorts membrane cargo for anterograde transport in the Golgi. *Dev. Cell.* **47**, 479–493.e7
26. Fukata, M., Fukata, Y., Adesnik, H., Nicoll, R. A., and Bredt, D. S. (2004) Identification of PSD-95 palmitoylating enzymes. *Neuron.* **44**, 987–996
27. Ohno, Y., Kihara, A., Sano, T., and Igarashi, Y. (2006) Intracellular localization and tissue-specific distribution of human and yeast DHHC cysteine-rich domain-containing proteins. *Biochim. Biophys. Acta.* **1761**, 474–483
28. Lemonidis, K., Werno, M. W., Greaves, J., Diez-Ardanuy, C., Sanchez-Perez, M. C., Salaun, C., *et al.* (2015) The zDHHC family of S-acyltransferases. *Biochem. Soc. Trans.* **43**, 217–221
29. Sobocińska, J., Roszczenko-Jasińska, P., Zareba-Kozioł, M., Hromada-Judycka, A., Matveichuk, O. V., Traczyk, G., *et al.* (2018) Lipopolysaccharide upregulates palmitoylated enzymes of the phosphatidylinositol cycle: an insight from proteomic studies. *Mol. Cell Proteomics.* **17**, 233–254
30. Sobocińska, J., Roszczenko-Jasińska, P., Ciesielska, A., and Kwiatkowska, K. (2018) Protein palmitoylation and its role in bacterial and viral infections. *Front. Immunol. J.* **19**, 2003
31. Hang, H. C., Geutjes, E. J., Grotenbreg, G., Pollington, A. M., Bijlmakers, M. J., and Ploegh, H. L. (2007) Chemical probes for the rapid detection of fatty-acylated proteins in mammalian cells. *J. Am. Chem. Soc.* **129**, 2744–2745
32. Martin, B. R., and Cravatt, B. F. (2009) Large-scale profiling of protein palmitoylation in mammalian cells. *Nat. Methods.* **6**, 135–138
33. Drisdell, R. C., Alexander, J. K., Sayeed, A., and Green, W. N. (2006) Assays of protein palmitoylation. *Methods.* **40**, 127–134
34. Roth, A. F., Wan, J., Bailey, A. O., Sun, B., Kuchar, J. A., Green, W. N., *et al.* (2006) Global analysis of protein palmitoylation in yeast. *Cell.* **125**, 1003–1013
35. Fukata, Y., Iwanaga, T., and Fukata, M. (2006) Systematic screening for palmitoyl transferase activity of the DHHC protein family in mammalian cells. *Methods.* **40**, 177–182
36. Ziemlińska, E., Sobocińska, J., Świątkowska, A., Hromada-Judycka, A., Traczyk, G., Malinowska, A., *et al.* (2021) Palm oil-rich diet affects murine liver proteome and S-palmitoylome. *Int. J. Mol. Sci.* **22**, 13094
37. Percher, A., Ramakrishnan, S., Thion, E., Yuan, X., Yount, J. S., and Hang, H. C. (2016) Mass-tag labeling reveals site-specific and endogenous levels of protein S-fatty acylation. *Proc. Natl. Acad. Sci. U. S. A.* **113**, 4302–4307
38. Hammond, G. R., Schiavo, G., and Irvine, R. F. (2009) Immunocytochemical techniques reveal multiple, distinct cellular pools of PtdIns4P and PtdIns(4,5)P₂. *Biochem. J.* **422**, 23–35
39. Dunn, K. W., Kamocka, M. M., and McDonald, J. H. (2011) A practical guide to evaluating colocalization in biological microscopy. *Am. J. Physiol. Cell Physiol.* **300**, C723–C742
40. Prymas, K., Świątkowska, A., Traczyk, G., Ziemlińska, E., Dziełulska, A., Ciesielska, A., *et al.* (2020) Sphingomyelin synthase activity affects TRIF-dependent signaling of Toll-like receptor 4 in cells stimulated with lipopolysaccharide. *Biochim. Biophys. Acta Mol. Cell Biol. Lipids.* **1865**, 158549
41. Collins, M. O., Woodley, K. T., and Choudhary, J. S. (2017) Global, site-specific analysis of neuronal protein S-acylation. *Sci. Rep.* **7**, 4683
42. Hofmann, K. (2000) A superfamily of membrane-bound O-acyltransferases with implications for Wnt signaling. *Trends Biochem. Sci.* **25**, 111–112
43. Resh, M. D. (2016) Fatty acylation of proteins: the long and the short of it. *Prog. Lipid Res.* **63**, 120–131
44. Perrody, E., Abrami, L., Feldman, M., Kunz, B., Urbé, S., and van der Goot, F. G. (2016) Ubiquitin-dependent folding of the Wnt signaling coreceptor LRP6. *Elife.* **5**, e19083
45. Locatelli, C., Lemonidis, K., Salaun, C., Tomkinson, N. C. O., and Chamberlain, L. H. (2020) Identification of key features required for efficient S-acylation and plasma membrane targeting of sprouty-2. *J. Cell Sci.* **133**, jcs249664
46. Hernandez, L. M., Montersino, A., Niu, J., Guo, S., Faezov, B., Sanders, S. S., *et al.* (2023) Palmitoylation-dependent control of JAK1 kinase signaling governs responses to neuropoietic cytokines and survival in DRG neurons. *J. Biol. Chem.* **299**, 104965
47. Kobayashi, N., Hozumi, Y., Ito, T., Hosoya, T., Kondo, H., and Goto, K. (2007) Differential subcellular targeting and activity-dependent subcellular localization of diacylglycerol kinase isozymes in transfected cells. *Eur. J. Cell Biol.* **86**, 433–444
48. Matsui, H., Hozumi, Y., Tanaka, T., Okada, M., Nakano, T., Suzuki, Y., *et al.* (2014) Role of the N-terminal hydrophobic residues of DGK ϵ in targeting the endoplasmic reticulum. *Biochim. Biophys. Acta.* **1842S**, 1440–1450
49. Abrami, L., Dallavilla, T., Sandoz, P. A., Demir, M., Kunz, B., Savoglidis, G., *et al.* (2017) Identification and dynamics of the human ZDHHC16-ZDHHC6 palmitoylation cascade. *Elife.* **6**, e27826
50. Kwiatkowska, K., Matveichuk, O. V., Fronk, J., and Ciesielska, A. (2020) Flotillins: at the intersection of protein S-palmitoylation and lipid-mediated signaling. *Int. J. Mol. Sci.* **21**, 2283
51. Luke, M. R., Houghton, F., Perugini, M. A., and Gleeson, P. A. (2005) The trans-Golgi network GRIP-domain proteins form α -helical homodimers. *Biochem. J.* **388**, 835–841
52. Patil, C. S., Li, H., Lavine, N. E., Shi, R., Bodalia, A., Siddiqui, T. J., *et al.* (2022) ER-resident STIM1/2 couples Ca²⁺ entry by NMDA receptors to pannexin-1 activation. *Proc. Natl. Acad. Sci. U. S. A.* **119**, e2112870119
53. Barbernitz, X., and Raben, D. M. (2022) Phosphorylation of DGK. *Adv. Biol. Regul.* **88**, 100941
54. Jiang, H., Zhang, X., Chen, X., Aramsangtienchai, P., Tong, Z., and Lin, H. (2018) Protein lipidation: occurrence, mechanisms, biological functions, and enabling technologies. *Chem. Rev.* **118**, 919–988
55. Lemonidis, K., Gorleku, O. A., Sanchez-Perez, M. C., Grefen, C., and Chamberlain, L. H. (2014) The Golgi S-acylation machinery comprises zDHHC enzymes with major differences in substrate affinity and S-acylation activity. *Mol. Biol. Cell.* **25**, 3870–3883
56. Greaves, J., Munro, K. R., Davidson, S. C., Riviere, M., Wojno, J., Smith, T. K., *et al.* (2017) Molecular basis of fatty acid selectivity in the zDHHC family of S-acyltransferases revealed by click chemistry. *Proc. Natl. Acad. Sci. U. S. A.* **114**, E1365–E1374
57. Lemonidis, K., Sanchez-Perez, M. C., and Chamberlain, L. H. (2015) Identification of a novel sequence motif recognized by the ankyrin repeat domain of zDHHC17/13 S-acyltransferases. *J. Biol. Chem.* **290**, 21939–21950
58. Verardi, R., Kim, J. S., Ghirlando, R., and Banerjee, A. (2017) Structural basis for substrate recognition by the ankyrin repeat domain of human DHHC17 palmitoyltransferase. *Structure.* **25**, 1337–1347.e6
59. Butler, L., Locatelli, C., Allagioti, D., Lousa, I., Lemonidis, K., Tomkinson, N. C. O., *et al.* (2023) S-acylation of Sprouty and SPRED proteins by the S-acyltransferase zDHHC17 involves a novel mode of enzyme-substrate interaction. *J. Biol. Chem.* **299**, 102754
60. Abrami, L., Kunz, B., Iacovache, I., and van der Goot, F. G. (2008) Palmitoylation and ubiquitination regulate exit of the Wnt signaling protein LRP6 from the endoplasmic reticulum. *Proc. Natl. Acad. Sci. U. S. A.* **105**, 5384–5389
61. Saheki, Y., Bian, X., Schauder, C. M., Sawaki, Y., Surma, M. A., Klose, C., *et al.* (2016) Control of plasma membrane lipid homeostasis by the extended synaptotagmins. *Nat. Cell Biol.* **18**, 504–515
62. Kim, Y. J., Guzman-Hernandez, M. L., Wisniewski, E., and Balla, T. (2015) Phosphatidylinositol-phosphatidic acid exchange by Nir2 at ER-PM contact sites maintains phosphoinositide signaling competence. *Dev. Cell.* **33**, 549–561
63. Kim, Y. J., Guzman-Hernandez, M. L., Wisniewski, E., Echeverria, N., and Balla, T. (2016) Phosphatidylinositol and phosphatidic acid transport between the ER and plasma membrane during PLC activation requires the Nir2 protein. *Biochem. Soc. Trans.* **44**, 197–201
64. Nakano, T., and Goto, K. (2022) Diacylglycerol kinase ϵ in adipose tissues: a crosstalk between signal transduction and energy metabolism. *Front. Physiol.* **13**, 815085
65. Sato, M., Liu, K., Sasaki, S., Kunii, N., Sakai, H., Mizuno, H., *et al.* (2013) Evaluations of the selectivities of the diacylglycerol kinase inhibitors R59022 and R59949 among diacylglycerol kinase

- isozymes using a new non-radioactive assay method. *Pharmacology*. **92**, 99–107
66. Barneda, D., Janardan, V., Niewczas, I., Collins, D. M., Cosulich, S., Clark, J., *et al.* (2022) Acyl chain selection couples the consumption and synthesis of phosphoinositides. *EMBO J.* **41**, e110038
67. Myeong, J., de la Cruz, L., Jung, S-R., Yeon, J-H., Suh, B-C., Koh, D-S., *et al.* (2020) Phosphatidylinositol 4,5-bisphosphate is regenerated by speeding of the PI 4-kinase pathway during long PLC activation. *J. Gen. Physiol.* **152**, e202012627
68. de Rubio, R. G., Ransom, R. F., Malik, S., Yule, D. I., Anantharam, A., and Smrcka, A. V. (2018) Phosphatidylinositol 4-phosphate is a major source of GPCR-stimulated phosphoinositide production. *Sci. Signal.* **11**, eaan1210